The Cross–Convolution Method for Interpreting SKS Splitting Observations, with Application to One and Two Layer Anisotropic Earth Models

William Menke
Lamont–Doherty Earth Observatory of Columbia University
and
Vadim Levin
Dept. of Geological Sciences, Rutgers University

Summary

We present a new method for determining anisotropic earth models using observations of split shear waves (such as SKS). The method consists of first constructing two timeseries, x(t) and y(t), that contain information about both the observed seismograms and a hypothetical earth model, and then varying the earth model so as to minimize the misfit, e(t)=x(t)–y(t). The timeseries are defined by the rules, $x(t)=h^{pre}(\mathbf{m},t)*V^{obs}(t)$ and $y(t)=v^{pre}(\mathbf{m},t)*H^{obs}(t)$, where $V^{obs}(t)$ and $H^{obs}(t)$ are the observed radial–horizontal and tangential–horizontal component seismograms, respectively, $v^{pre}(\mathbf{m},t)$ and $h^{pre}(\mathbf{m},t)$ are the radial–horizontal and tangential–horizontal impulse responses, respectively, predicted by some earth model, **m**, and * denotes convolution. The best–fitting earth model is the one that minimizes $||e(t)||^2$ with respect to **m**, where ||.|| is an amplitude–normalized L_2 norm. This definition of misfit is insensitive to the source wavelet, and thus eliminates that unknown quantity from the problem. We show that this method yields estimates of one–layer splitting parameters that are very similar to those achieved through traditional means, but that unlike those traditional methods it can be applied to more complicated models (e.g. multi–layer anisotropy) without recourse to approximate "apparent splitting" parameters. We apply the method to synthetic SKS pulses generated for two–layer

anisotropic earth models, and show that it can successfully recover information about both layers. We then apply the method to SKS and PKS data from PFO (Piñon Flat, California) on the San Andreas fault. This station has been studied previously by Őzalaybey and Savage (1995), Liu et al. (1995) and Polet and Kanamori (2002), who provide two–layer solutions based on modeling of the azimuthal variation of apparent splitting parameters. Our results are broadly consistent with theirs, but provide additional information about the statistical significance of the two–layer solution. By this measure, neither solution is significantly better than a one–layer solution, although all fit the waveform data better than the best–fitting one layer solution. This result is consistent with the interpretations of Őzalaybey and Savage (1995) and Liu et al. (1995), who provide similar assessments of the their two–layer solutions. The fact that neither our one–layer nor two–layer solutions does very well at reducing the overall misfit strongly suggests that some process other than two–layer anisotropy is affecting SKS and PKS waveforms at PFO.

Introduction

The Earth is anisotropic to seismic wave propagation on a broad range of scales, from the scale of the whole earth (as measured, say, by normal mode oscillations) (Anderson & Dziewonski, 1982) to the scale of rock handsamples (due to petrofabrics) (Ben Ismail and Mainprice, 1998). In the shallow crust, anisotropy may reflect systems of fluid–filled cracks and sedimentary layers with alternating velocities (Babuška and Cara, 1991). At depths where cracks close due to lithostatic pressure, anisotropy is likely due to interlayering of rocks with different properties,

e.g. caused by intrusion of dikes (Holliger and Levander, 1994) as well as to intrinsic anisotropy of foliated metamorphic rocks such as metapelites (Burlini and Fountain, 1998). Systematic orientation of olivine crystals by deformation (Zhang and Karato, 1995) is a dominant cause of anisotropy in the upper mantle. Anisotropy within and below the transition zone, and at the core–mantle boundary have been proposed (Montagner, 1998; Kendall and Silver, 1998), although mechanisms remain enigmatic. Finally, the inner core of the planet is anisotropic, most likely due to systematic arrangement of constituent iron crystals (Creager, 2000).

Upper–mantle seismic anisotropy is thought mainly to be caused by systematic alignment of olivine crystals ("lattice preferred orientation", LPO) and is thus related to mantle deformation processes. It is of particular interest due to its likely connection with past and present geodynamic processes (Vinnik et al, 1992; Silver, 1996; Park and Levin, 2002). The shear–wave splitting technique stands out among methods designed to detect upper–mantle anisotropy because of ease of use and potentially powerful interpretations (Savage, 1999). The technique is based upon the behavior of a shear wave, which splits into two components as it propagates through an anisotropic medium. One component is polarized in the plane of the "fast" direction of the anisotropic material, and propagates with a relatively fast velocity. The other component is polarized in the orthogonal plane (the"slow" direction), and propagates with a relatively slow velocity. A common method of quantifying the effect of anisotropy on a shear wave is to determine its two "splitting parameters", ϕ and τ. The parameter ϕ denotes the azimuth of the polarization of the "fast" shear wave. In olivine–dominated mantle rocks the fast direction is the preferred orientation of

alignment for the “a” axes of olivine crystals (Christensen, 1984; Ben Ismail and Mainprice, 1998). The orientation of this crystalographic axis reflects, to the first order, the direction of solid flow in the material (Zhang and Karato, 1995; Kaminsky and Ribe, 2001). The parameter, τ, is the time delay between the “fast” and the “slow” components. The value of τ serves as a rough measure of the thickness for the anisotropic region sampled by a subvertical raypath. Assuming an average anisotropy of 4% (Silver, 1996), a τ of 1s roughly corresponds to a 100 km thick anisotropic layer.

Core–refracted teleseismic shear waves (SKS, SKKS, PKS and similar phases) are especially useful since they are affected by anisotropy only on the “receiver–side” of their path. Their passage across the core–mantle boundary removes "source–side" splitting. Furthermore, they have a known initial polarization. At the start of their ascent from the core–mantle boundary these phases are purely radially–polarized, with particle motion in the vertical plane of the source and receiver. Finally, they ascend almost vertically through the mantle, and thus sample upper–mantle anisotropy at near–normal incidence, which is simpler to interpret than a shallow angle.

The splitting parameter method was initially developed for application to long–period seismic data (Vinnik et al, 1984; Silver and Chan, 1988), and makes 2 significant assumptions about the mechanism of anisotropy: 1) that only one anisotropic symmetry system is present along the path; and 2) that two of the 3 symmetry axes

are in the horizontal plane. The first assumption is due to the fact that a splitting parameter is only well defined when the one symmetry is present. The second assumption is needed to justify the averaging of a set of splitting parameters, determined for different angles of incidence and backazimuths, into a single splitting determination. It can be relaxed if the individual measurements are used as input to an inversion for a best-fitting anisotropic tensor (Savage 1999). The method is relatively insensitive to the type of symmetry (e.g. hexagonal or orthorhombic). A direct outcome of the above assumptions is the uniformity of shear–wave splitting parameters, ϕ and τ , expected for observations from any direction (say, as quantified by the backazimuth to the source), as long as all shear waves have near–normal incidence. This expectation is sometimes not born out by actual observations when a broad range of directions is sampled. Instead, significant variation of observed shear–wave splitting parameters with direction is observed (e.g., Silver and Savage, 1994; Őzalaybey and Savage, 1995; Levin et al, 1999; Hartog and Schwartz, 2000).

Violation of either of the initial assumptions about the structure of anisotropy along the path leads to the expectation that the fast axis, θ, and delay, τ, vary with backazimuth, ϕ. (Rumpker and Silver, 1998; Levin et al., 1999; Saltzer et al, 2000; Hartog and Schwartz, 2000). Figure 1 demonstrates how parameters of shear–wave birefringence measured in the expectation of a single symmetry axis depend on the direction of the incoming wave if two different anisotropic systems are sampled instead. Except for special case of wave propagation exactly along the symmetry axis of one of the layers in the medium, each pair of (θ, τ) values reflects contribution

from both. It is therefore inaccurate to relate individual measurements directly to the anisotropic structure along the path. Rather, these (θ, τ) pairs may be thought of as "apparent" splitting parameters, with the implication that they must be examined in the context of their directional behaviour (e.g., Saltzer et al., 2000).

Commonly, strategies for resolving depth-dependent and/or non-horizontal anisotropic structure from shear-wave splitting observations utilize systematics in the variation of apparent splitting parameters with backazimuth to infer anisotropic properties. Analytic expressions describing direction systematics may be derived for layered structures with hexagonal symmetry of anisotropy and horizontal axes (Silver and Savage, 1994; Rümpker and Silver, 1998; Saltzer et al., 2000). Alternatively, synthetic seismogram computations may be performed in a set of trial models, with subsequent visual evaluation of resulting waveforms and estimation of shear wave splitting parameters (e.g., Levin et al., 1999, Hartog and Schwartz, 2001). Another approach, by Ozalaybey and Savage (1994), was to find an analytic splitting operator that would "remove" the effects of two anisotorpic layers from observed waveforms. Like its parent technique, the splitting operator method of Silver and Chan (1991), this approach has the mechanism of waveform perturbation built in.

This paper develops a more general methodology that is not based on apparent splitting parameters, and does not contain prior assumptions about the process affecting the waveforms We show that it is possible to interrogate waveforms of individual shear waves for evidence of complex anisotropy being present along their path. Our approach here is to develop a data analysis method that assesses whether seismic waveforms are consistent with a particular one–layer or multi–layer

anisotropic earth model. We are motivated by what we see as a flaw in approaches that rely upon measurements of apparent splitting parameters. These methods force a fit to a simple one–layer model that might very well be poor, and which in any case may be insensitive to important features in data that don't fit a one–layer model. In moving away from apparent splitting measurements, we must set aside an insight that was important in the early development of the field, namely that anisotropy can be recognized by the presence of two waveforms of the same shape, with perpendicular polarization and one delayed with respect to the other. Instead, we must recognize that when complicated anisotropy is present, the wavefield is itself complicated and no simple set of parameters can adequately describe that complication. Our approach then is to apply a standard waveform–matching procedure, to first assess whether the predictions of a given anisotropic earth model is consistent with a given shear–wave splitting dataset, and second, to use that assessment as part of a systematic model–fitting exercise that determines a best–fit anisotropic model.

The general idea of minimizing an error associated with mismatched seismic waveforms is inherent in most splitting-parameter estimation techniques, such as Silver and Chan's (1991). What is new here is our way of defining that error so that the method can be generalized to multilayered media. Of course, if we were willing to compute complete synthetic seismograms that could be compared with the data, we could use existing waveform inversion methods (e.g. Mellman 1980) to invert for anisotropy. However, the calculation of complete synthetic seismograms is time–consuming and requires information about the earthquake, such as its focal mechanism and source time function, that are often unknown. The method we

describe here does not require source information.

Methodology

Suppose that a seismic station detects several teleseismic phases, such as SKS, from a variety of sources with different angles of incidence and azimuths. Let the radial–horizontal and tangential–horizontal seismograms be denoted, $V_i^{obs}(t)$, and, $H_i^{obs}(t)$, respectively. Here the subscript, i, indexes the N phases. We assume that these seismograms have been windowed to isolate the phase of interest. We can represent each seismogram as the convolution of a "source" wavelet, $s_i(t)$, with the radial and tangential impulse response functions, $v_i(t)$ and $h_i(t)$. These response functions quantify the effect of near–receiver structure on the phase:

$$V_i^{obs}(t) = s_i^{true}(t) * v_i^{true}(t) \qquad \text{(Eqn. 1)}$$
$$H_i^{obs}(t) = s_i^{true}(t) * h_i^{true}(t) \qquad \text{(Eqn. 2)}$$

We use the superscript "true" to indicate that in the absence of noise the observed seismograms are related to the actual source wavelet and impulse responses. The term, s(t), is a "source" wavelet in the sense that it characterizes the waveform of the phase before it interacts with the near–receiver structure. It describes both the effects of the earthquake source itself and subsequent modification by structure far from the receiver. An important aspect of these equations is that the same source wavelet appears in both equations.

Suppose that we have a model, **m**, for the near–receiver earth structure. Here the vector, **m**, denotes whatever parameters might be needed to define that model. For

example, in the simple case of one–layer anisotropy, $\mathbf{m}=[\tau,\theta]^T$, would represent the splitting delay, τ, and azimuth, θ, of the fast anisotropic axis. In more complicated cases it might include additional parameters that describe additional anisotropic layers, crustal thickness, interface dip, etc. We assume that a method of predicting the impulse responses $v_i^{pre}(\mathbf{m},t)$ and $h_i^{pre}(\mathbf{m},t)$ of the earth model, **m**, is available. Then the predicted seismograms are:

$$V_i^{pre}(t) = s_i^{true}(t) * v_i^{pre}(\mathbf{m},t) \qquad \text{(Eqn. 3)}$$
$$H_i^{pre}(t) = s_i^{true}(t) * h_i^{pre}(\mathbf{m},t) \qquad \text{(Eqn. 4)}$$

Here the superscript, "pre", stands for "predicted". We would now like to select a model, **m**, that best matches the predicted seismograms to the observed ones. The presence of the source wavelet term in these equations is an impediment to this goal, since it is, in general, unknown.

We pursue the following strategy for removing the source wavelet from these equations: Convolve Eqn. 1 by $h_i^{pre}(\mathbf{m},t)$ and Eqn. 2 by $v_i^{pre}(\mathbf{m},t)$:

$$h_i^{pre}(\mathbf{m},t) * V_i^{obs}(t) = s_i^{true}(t) * v_i^{true}(t) * h_i^{pre}(\mathbf{m},t) \qquad \text{(Eqn. 5)}$$
$$v_i^{pre}(\mathbf{m},t) * H_i^{obs}(t) = s_i^{true}(t) * h_i^{true}(t) * v_i^{pre}(\mathbf{m},t) \qquad \text{(Eqn. 6)}$$

If the model, **m**, is a good one, we ought to have $v_i^{pre}(\mathbf{m},t) \approx v_i^{true}(t)$ and $h_i^{pre}(\mathbf{m},t) \approx h_i^{true}(t)$. The right hand sides of Eqns. 5 and 6 are then approximately equal. By equating the left hand sides we find that:

$$h_i^{pre}(\mathbf{m},t) * V_i^{obs}(t) \approx v_i^{pre}(\mathbf{m},t) * H_i^{obs}(t) \qquad \text{(Eqn. 7)}$$

Least–squares minimization of the error in Eqn. 7 can now be used to find an estimate of the model:

find the $\mathbf{m}^{est}$ that minimizes
$E(\mathbf{m}) = (1/N)\ \Sigma_{i=1}^{N} \| h_i^{pre}(\mathbf{m},t) * V_i^{obs}(t) - v_i^{pre}(\mathbf{m},t) * H_i^{obs}(t) \|^2$
with respect to $\mathbf{m}$ (Eqn. 8)

Here the superscript "est" denotes "estimated" and $\|.\|^2$ denotes some measure of the difference between the two timeseries. One possible choice is:

$$\|x_i(t)-y_i(t)\|^2 = \int [x_i(t)-y_i(t)]^2\, dt \,/\, [\int x_i^2(t)dt + \int y_i^2(t)dt] \qquad \text{(Eqn. 9)}$$

Here $x_i(t)=h_i^{pre}(\mathbf{m},t)*V_i^{obs}(t)$ and $y_i(t)=v_i^{pre}(\mathbf{m},t)*H_i^{obs}(t)$. Eqn. 9 is based on the commonly–used L_2 norm, and has been normalized so that the terms in Eqn. 8 are of similar size (i.e. all phases are treated equally, regardless of the overall amplitude of the seismograms). The misfit, $E(\mathbf{m})$, is zero if all the seismograms are exactly matched and is of order unity if all the fits are poor.

The special case of an isotropic material needs discussion. In the absence of noise, both the observed tangential–component seismograms, $H_i^{obs}(t)$, and the timeseries, $y_i(t)$, are exactly zero. The best fitting model is obtained by minimizing $\Sigma_{i=1}^{N} \|x_i(t)\|$, which is to say by choosing the model, $\mathbf{m}$, such that $h_i^{pre}(\mathbf{m},t)=0$ for all i. This procedure correctly selects the isotropic model. However, when noise is present, it will tend to select an anisotropic model that 'fits the noise'. This case can be recognized by testing the statistical significance of the error reduction. Alternatively, one could use a different coordinate system (i.e., north and east instead of radial and tangential) that doesn't suffer from this problem.

We will refer to this procedure for determining near–receiver structure from seismic

waveforms as the "cross–convolution method". It has a close relationship to procedures commonly used to interpret "receiver functions" (Phinney 1964, Burdick and Langston 1977), which are used to recover crustal and upper mantle layering. The receiver function method typically uses vertical and radial–horizontal component seismograms of a P wave and its reverberations, not the radial and tangential components of SKS that are used here to infer anisotropy. This difference can be accommodated by re–identifying v(t) and V(t) with the vertical component, and h(t) and H(t) with the radial–horizontal component. Then the receiver function method begins by solving Eqns. 1 and 2 for the source wavelet:

$$s_i^{true}(t) = V_i^{obs}(t) * v_i^{-1true}(t) = H_i^{obs}(t) * h_i^{-1true}(t) \qquad \text{(Eqn. 10)}$$

Here $v^{-1}{}_i^{obs}(t)$ and $h^{-1}{}_i^{obs}(t)$ are the inverse functions to $V_i^{obs}(t)$ and $H_i^{obs}(t)$, respectively, in the sense that $v^{-1}{}_i^{obs}(t)*v_i^{obs}(t)=h^{-1}{}_i^{obs}(t)*h_i^{obs}(t)=\delta(t)$, where $\delta(t)$ is the Dirac delta function). The equality in Eqn. 10 is then rearranged to yield:

$$h_i^{true}(t) * v^{-1}{}_i^{true}(t) = H_i^{obs}(t) * V^{-1}{}_i^{obs}(t) = R_i(t) \qquad \text{(Eqn. 11)}$$

The observed receiver function, $R_i^{obs}(t)$, can be constructed by deconvolving one of the observed seismogram components from the other: $R_i^{obs}(t)=H_i^{obs}(t)*V^{-1}{}_i^{obs}(t)$. It can be compared with a receiver function, $R_i^{pre}(\mathbf{m},t)=h_i^{pre}(\mathbf{m},t)*v^{-1}{}_i^{pre}(\mathbf{m},t)$, predicted from some earth model, **m**. Once again, least–squares can be used to select a best–fitting model:

find the $\mathbf{m}^{est}$ that minimizes
$E(\mathbf{m}) = \Sigma_{i=1}^{N} \| R_i^{obs}(t) - R_i^{pre}(\mathbf{m},t) \|^2$
with respect to **m** (Eqn. 12)

The cross–convolution method that we develop here and apply to estimating anisotropy from split shear waves can equally well be applied to determining isotropic layering from P wave coda, and is thus an alternative to traditional receiver function analysis. A major advantage of this cross–convolution method over the receiver function method is that no deconvolution need be performed. Deconvolution is undesirable because it suffers from instability when the timeseries are band–limited. Furthermore, it avoids the embarrassing problem that not every conceivable layered earth model has a well–defined receiver function (i.e., the receiver function is singular if the spectrum of $v_i(t)$ has a zero).

Application to One and Two Layer Anisotropy

Suppose that a radially–polarized phase, such as SKS, traverses a single anisotropic layer located beneath the source. Furthermore, suppose that the anisotropy is "azimuthal", in the sense that the fast axis is horizontal, with an azimuth, θ. Then the impulse response of the layer to a normally–incident shear wave from below is approximately:

$$v_i^{pre}(\mathbf{m},t) = a_1\ \delta(t) + a_2\ \delta(t-\tau)$$
$$h_i^{pre}(\mathbf{m},t) = b_1\ \delta(t) + b_2\ \delta(t-\tau)$$

$$a_1 = \cos^2(\theta-\phi)$$
$$a_2 = \sin^2(\theta-\phi)$$
$$b_1 = -b_2 = \cos(\theta-\phi)\sin(\theta-\phi)$$

(Eqn. 13)

Here we have defined the radial–horizontal direction to point back towards the source

and the tangential–horizontal direction to be 90° counterclockwise from the radial–horizontal direction, and the azimuth of the radial direction (i.e., the backazimuth of the source) to be ϕ. The fast shear wave arrives at the station at time, t=0, and the slow shear wave is delayed by a splitting time, τ. This model has two parameters, $\mathbf{m}=[\tau,\theta]^T$. Note that the application of this formula to actual SKS phases is only approximate, since their propagation path is not exactly vertical. While this problem could be corrected by using a more complicated formula than Eqn. 13, the approximation will later be shown to be sufficiently accurate for the analysis given here.

If the station were underlain by two anisotropic layers, then the impulse response would be:

$$v_i^{pre}(\mathbf{m},t) = a_1\,\delta(t) + a_2\,\delta(t-\tau_2) + a_3\,\delta(t-\tau_1) + a_4\,\delta(t-\tau_1-\tau_2)$$
$$h_i^{pre}(\mathbf{m},t) = b_1\,\delta(t) + b_2\,\delta(t-\tau_2) + b_3\,\delta(t-\tau_1) + b_4\,\delta(t-\tau_1-\tau_2)$$

$$a_1 = \cos^2(\theta-\phi)\cos^2(\psi-\phi) + \cos(\theta-\phi)\sin(\theta-\phi)\cos(\psi-\phi)\sin(\psi-\phi)$$
$$a_2 = \cos^2(\theta-\phi)\sin^2(\psi-\phi) - \cos(\theta-\phi)\sin(\theta-\phi)\cos(\psi-\phi)\sin(\psi-\phi)$$
$$a_3 = \sin^2(\theta-\phi)\cos^2(\psi-\phi) - \cos(\theta-\phi)\sin(\theta-\phi)\cos(\psi-\phi)\sin(\psi-\phi)$$
$$a_4 = \sin^2(\theta-\phi)\sin^2(\psi-\phi) + \cos(\theta-\phi)\sin(\theta-\phi)\cos(\psi-\phi)\sin(\psi-\phi)$$

$$b_1 = \cos^2(\theta-\phi)\cos(\psi-\phi)\sin(\psi-\phi) + \cos(\theta-\phi)\sin(\theta-\phi)\sin^2(\psi-\phi)$$
$$b_2 = -\cos^2(\theta-\phi)\cos(\psi-\phi)\sin(\psi-\phi) + \cos(\theta-\phi)\sin(\theta-\phi)\cos^2(\psi-\phi)$$
$$b_3 = \sin^2(\theta-\phi)\cos(\psi-\phi)\sin(\psi-\phi) - \cos(\theta-\phi)\sin(\theta-\phi)\sin^2(\psi-\phi)$$
$$b_4 = -\sin^2(\theta-\phi)\cos(\psi-\phi)\sin(\psi-\phi) - \cos(\theta-\phi)\sin(\theta-\phi)\cos^2(\psi-\phi)$$

(Eqn. 14)

The model has four parameters, $\mathbf{m}=[\tau_1,\theta,\tau_2,\psi]^T$, with the bottom layer having splitting delay time, τ_1, and a fast axis with azimuth, θ, and the top layer having splitting delay time, τ_2, and fast axis with azimuth, ψ. As before, this model assumes normal incidence.

We use an exhaustive grid search to solve both the one–layer and two–layer problems. This approach is computationally intensive, but avoids the problems associated with linearized inversions (e.g. mistaking local minima in E(**m**) for the global minimum). We use a five–degree sampling interval on the interval 0–180° for angles and 0.1s for splitting delay on the interval 0–5s, so that about E(**m**) need be evaluated about 36×50=1800 times for 1–layer models and about $(36\times50)^2 \approx 3\times10^6$ for 2–layer models. The one–layer problem (2 model parameters) can be solved relatively rapidly (i.e. a few CPU–minutes on a fast workstation). The two–layer problem (4 model parameters) takes much longer (about a CPU–day). We note that the grid–search algorithm is highly parallelizable, so these computation times could be very significantly reduced on a computer with multiple processors.

More complicated models are, of course, plausible. One could allow a more complicated form of anisotropy, say with a dipping fast axis, in which case the dip would be a model parameter. And one could include a horizontal or dipping surface layer that modeled crustal reverberations. A linearized inversion would probably be necessary to solve such problems, given the larger number of model parameters.

Note that both the one–layer and two–layer impulse response functions (Eqns. 13 and 14) have the same form. They both consists of a small number (say, L) of spikes, with the spikes occurring at the same times on both the radial and tangential components:

$$v_i^{pre}(\mathbf{m},t) = \Sigma_{j=1}^{L} a_j \ \delta(t-T_j)$$
$$h_i^{pre}(\mathbf{m},t) = \Sigma_{j=1}^{L} b_j \ \delta(t-T_j) \qquad \text{(Eqn. 15)}$$

Here a_j and b_j are the amplitudes of the spikes and T_j is their time of occurrence. Note T_1 can be taken to be zero, and L is twice the number of layers. Instead of viewing the coefficients, $a_j(\mathbf{m})$ and $b_j(\mathbf{m})$ as functions of the model, **m** (as we do above), we could instead consider them as model parameters and solve for them (along with the times, T_j) directly. This approach places fewer preconceptions on the form of impulse response functions, and provides a way of examining whether, for example, the best–fitting coefficients really vary with backazimuth, ϕ, in the way predicted by Eqns. 13 or 14. For instance, in the one–layer case we could test whether:

$$-b_2/b_1=1$$
and
$$b_1/(a_1^2+a_2^2)^{1/2}=\cos(\theta-\phi)\sin(\theta-\phi) \qquad \text{(Eqn. 16)}$$

as predicted by Eqn. 13.

The least–squares estimation problem for (a_j, b_j, T_j) in Eqn. 15 has 3L–1 unknowns (i.e. 5 for the 1–layer case and 11 in the 2–layer case), larger than for the Eqs. 13 and 14 (2 for the 1–layer case and 4 for the 2–layer case). However, the larger number of unknowns is offset by an underlying simplicity of the structure of the problem: For any given set of pulse times, T_j, the problem of finding the best–fitting coefficients, a_j and b_j, is completely linear, and only requires solving a small (2L×2L) matrix equation for the a_j and b_j (Menke, 1989, Section 12.2). (Actually, the constraint $\Sigma_{j=1}^{L} a_j=1$ must also be included, since Eqn. 11 places no requirements on the absolute amplitude of the impulse response). The problem can be solved by a grid search over the (L–1) pulse times, T_j, alone. Our experience is that solutions up to about L=5 are practical.

Test on Synthetic Data

We construct two simple earth models, one with a single anisotropic layer in the upper mantle, and the other with 2 such layers. Each model has a 30 km thick isotropic crust, with a shear velocity of 3.76. km/s, overlaying an anisotropic mantle. The 1–layer model has a mantle consisting of a single anisotropic layer of 8% anisotropic peridotite, with a thickness of 100 km, a mean compressional velocity of 4.56 km/s, a fast axis azimuth of ϕ=112° and a splitting delay of 2.2s. The two–layer model has two anisotropic mantle layers of equal 100 km thickness, but with a lower layer with an azimuth of ϕ_1=68° and an upper layer with an azimuth of ϕ_2=112°.

We then computed synthetic seismograms for a receiver on the free surface of each model from SKS waves from a suite of backazimuths at 5° increments, all with a horizontal phase velocity of 20 km/s. We used the SPLITTING MODELER software (Menke 2000) to calculate the exact impulse response (i.e., including free surface effects and internal multiples), and then convolved them with a long–period (5s) source wavelet. Sample seismograms are shown in Figs. 2A and 3A. We then estimated the anisotropic model parameters from these seismograms.

The one–layer estimator (i.e. based on Eqn. 13) performs well, both when applied to individual seismograms (i.e. N=1 in Eqn. 8) or to the whole suite of backazimuths (i.e. N=37) (Fig. 4). The solutions account for about 99% of the error, with the residual 1% being mainly due to the unmodelled crustal reverberation (Fig 2B). The estimated fast axis azimuth agrees with the true value to within a degree. The

estimated delay time time also agrees with the true delay time, but shows some systematic scatter of about ±0.4s. This scatter correlates well with the shape of the minimum in the whole–suite error, E(**m**) (Fig. 5). The accuracy of these results justify the use of the approximate impulse response of Eqn. 13, which omits crustal reverberations and which assumes normal incidence.

The two–layer estimator (i.e. based on Eqn. 14) also performs well, both when applied to individual seismograms (i.e. N=1) and to the whole suite (i.e. N=37) (Fig. 6). The solutions account for about 99% of the error, with the residual 1% again being due to the unmodelled crustal reverberations (Fig 3C). The estimated azimuths of the fast axes agree with the true values to within a degree. The estimated delay time also agrees with the true delay times, again with systematic scatter of about ±0.4s. The error surface is shown in Fig. 7.

When the one–layer estimator is applied to the two–layer data, the overall fit is much poorer, with error reduction only in the 30–60% range (Fig. 3B). The estimated single–seismogram azimuth fluctuate strongly with backazimuth (Fig. 8). This "sawtooth" pattern has been noted previously by other authors (Silver and Savage, 1994; Rümpker and Silver, 1998; Saltzer et al., 2000) using "apparent spliting parameter" based methods, and cited as evidence for multiple anisotropic layers. The estimates for individual seismograms scatter significantly far from the minimum of the whole–suite error, E(**m**) (Fig 9).

Finally, we compute general, two–pulse operators and perform the two tests of Eqn

16. The results show that the best–fitting two–pulse response functions have the properties expected of one–layer anisotropic impulse response functions (Fig. 10). We thus have further confidence that the contribution of unmodelled processes (e.g. interface dip) is small.

Nonuniqueness of Two–Layer Estimates

If the data are in fact consistent with a one–layer model, then an interesting non–uniqueness arises when they are fit with a two layer model. This effect is associated with the fact that two layers of equal thickness and "crossed" polarization do not split normally–incident shear waves, regardless of their initial polarization. When the slow axis of one layer is exactly aligned with the fast axis of the other (and vice versa), then the components of the shear wave in these directions have exactly the same net traveltime through the layers. No net splitting occurs; all splitting from the first layer is undone by the second. Thus if the data are consistent with a single layer solution, $\mathbf{m}^{(1)}=[\tau, \theta]^T$, then they are also equally consistent with the two–layer solution, $\mathbf{m}^{(2)}=[\tau+\alpha, \theta, \alpha, \theta+\pi/2]^T$ and also with the different two–layer solution, $\mathbf{m}^{(2)}=[\alpha, \theta+\pi/2, \tau+\alpha, \theta]^T$, where α is an arbitrary delay time. In other words, one layer can be made arbitrarily thicker, if one chooses the polarization of the other layer to "cancel out" the increase.

Suppose now that the data are consistent with a one–layer model, $\mathbf{m}^{(1)}=[\tau, \theta]^T$, but that they also contain noise. It is entirely possible that a two–layer solution that is close to $\mathbf{m}^{(2)}=[\tau+\alpha, \theta, \alpha, \theta+\pi/2]^T$ or $\mathbf{m}^{(2)}=[\alpha, \theta+\pi/2, \tau+\alpha, \theta]^T$ will have smaller

error than the best–fitting one layer solution. The reduction in error would not be significant; the two–layer solution has merely fit the noise. This "nearly one–layer" two–layer solution can be recognized by having two dissimilar delays and fast axes that are nearly 90° apart.

This type of nonuniqueness does not arise if the data really are consistent with a two layer model, as long as the fast directions are not 90° apart, since the azimuths of both layers would be constrained by the data and could not be "crossed". It would arise, however, if the two–layer data were fit with a three–layer model.

Application to Piñon Flat (PFO) Seismic Station

To test the performance of our new method on a real data set, we chose station PFO (Piñon Flat, California), near the San Andreas fault in southern California, that has recorded over a decade of broadband digital data.

Shear wave splitting observations at this station have been reported by Liu et al. (1995), by Özalaybey and Savage (1995) and by Polet and Kanamori (2002). Only Liu et al. (1995), by Özalaybey and Savage (1995) report single–layer solutions. Their studies found similar single layer solutions for the splitting data, with ϕ ~90º and τ of 1.2 and 1.45 sec, respectively. While Polet and Kanamori (2002) do not give a specific one–layer solution, their Figure A2 indicates about 1s of splitting at PFO, with a more–or–less east–west direction . It is thus generally compatible with the other studies. The results of the three studies diverge in estimating 2–layer solutions

to the data available at the time, and none reported a strong preference for the 2–layer solution in terms of data fit.

By adding data from five more years of observations (1992–1999) we were able to assemble a data set with broader coverage, and could use only the larger, clearer events. Our dataset contains 41 seismograms of SKS and PKS phases (Fig. 11)observed at PFO for a broad suite of backazimuths (Fig. 11, inset and Table 1). The broadband data was bandpass filtered between 0.01 and 0.1 Hz, windowed to exclude extraneous phases, decimated to 10 samples/s and rotated to radial and tangential components.

We first compare the cross–convolution method to several other commonly–used methods of determining splitting parameters. The first of these relies on the assumption that the SKS wave is radially–polarized before it traverses the anisotropic region. The radial direction is known, because it is assumed to be given by the backazimuth. A good choice of anisotropic parameters is therefore one that minimizes the energy on the tangential component, once the predicted effect of the anisotropy is removed. We will call this the "Minimum tangential, fixed initial polarization" method (Method A).

One possible problem with this method is that lateral heterogeneity far from the receiver might deflect the initial polarization of the SKS wave away from the radial direction. While the SKS wave may still be linearly polarized, its polarization direction would not be exactly the radial direction. This possibility can be taken into

account simply by removing the predicted effect of anisotropy, and solving for the best–fitting direction of linear polarization. The best–fitting splitting parameters minimize the energy on the other, orthogonal horizontal component. We will call this the "Minimum tangential, variable initial polarization" method (or Method B).

Another method relies on the fact that if the initial polarization is linear, then in a rotated coordinate system parallel to the anisotropic axes, the pulse shapes at the receiver have exactly the same shape, but are delayed with respect to one another. The best–fitting splitting parameters are therefore those that maximize the cross–correlation of the rotated components. We will call this the "Maxmum cross–correlation" method (or Method C).

Both the "minimum tangential, variable initial polarization" and "maximum cross correlation" methods make no assumption about the orientation of the initial polarization, and both determine that direction as part of the solution process (Fig. 12). These resulting estimates can be compared to the backazimuth direction. For SKS, any disagreement may reflect noise, phase misidentification or mantle heterogeneity.

One–layer solutions, computed by each of these methods, as well as the new cross–convolution method (Method D) are shown in Table 2 and Fig. 13. The whole–suite solutions determined by the different methods are all reasonably consistent with one another, and with the values published by Őzalaybey & Savage (1995) and Liu et al, (1995). The estimated delay time ranges from 0.9 to 1.5 s, and the estimated fast axis

azimuth from 75–89°.

The individual–seismogram estimates show much greater variability. The variablity in fast azimuth is associated with “sawtooth” pattern of variation with backazimuth. This pattern is discernible for all methods, but is most pronounced for Method C (Fig. 14). Methods A, B, and D tend to have individual delays biased to larger values than the whole–suite estimate, while Method C tends to have individual delays biased to smaller values.

We have computed general two–pulse operators for the individual SKS waves, using the technique described in Eqn. 15, and used them to assess the degree to which the general operators behave like the one–layer anisotropic ones (i.e. by evaluating Eqn. 16) (Fig. 15). The results are poor, with large scatter about the expected pattern. This result indicates that the SKS seismograms contain significant features that cannot be explained by the simple one–layer model. This conclusion is supported by the fact that the overall variance reduction (with respect to the no–anisotropy case) of the various one–layer estimates is rather poor: 16%, 23%, 8%, and 55% for methods A, B, C, and D, respectively. We have examined selected individual seismograms by eye. Most have a significant tangential–component pulse that coincides with what is clearly the SKS pulse on the radial component, and which cannot therefore be “ground noise”. On the other hand, its shape is not always what one would expect from a simple one–layer model. Some other, unmodelled process is also occurring.

The two–layer cross–convolution method provides a unique two–layer solution (Table 3), but the overall variance reduction, when compared to the result of the one–layer method, is small (only 3.7%). This is in contrast to the synthetic example above, where the variance reduction is much larger – about 93%. In order to apply the F–test to estimate the significance of this error reduction, we need to estimate the number of degrees of freedom of the two estimates. The one–layer estimate is based on 41 seismograms, each with two components of 1000 samples, a bandwidth of 2.5% and two model parameters, so it has ν_1=2048 degrees of freedom. The two–layer estimate is based on the same data, but has four model parameters, so ν_2=2046. After consulting a table of the F–distribution, we find that the level of significance is about 80%, considerably less than the 95% standard that is commonly applied in judging significance. Therefore the fit of the two–layer model is not significantly better than the fit of the one–layer model.

The best–fit two–layer cross–convolution solution has a bottom layer with properties similar to those in the two–layer models published by Őzalaybey & Savage (1995) and Polet and Kanamori (2002), which are based on fitting the azimuthal variability in parameters estimated by a one–layer method similar to our Method A. The upper layer, however, is significantly different, and is somewhat thicker. The best–fit cross–convolution solution has two layers of rather unequal thicknesses and axes that are 83° apart. It is therefore of the “nearly one–layer” variety discussed in the previous section.

Őzalaybey & Savage's (1995) solution has smaller error, as judged by the cross convolution method, than the one–layer solution (Fig. 16). Furthermore, when the fast direction values are constrained equal to Őzalaybey & Savage's, the cross–convolutional method predicts delay times that are similar to Őzalaybey & Savage's (see "sub optimal" solution #1 in Table 3). This similarity indicates the Őzalaybey & Savage's methodology, which is based on interpreting the backazimuthal behavior of apparent splitting parameters, is indeed modeling some of the underlying anisotropic behavior of the wavefield. A similar exercise for the solution of Liu et al., (1995) yields estimates of delays in the lower and upper layers of 1.4 and 0.2 sec, respectively (Table 3). This differs from their reported values. However, given that fast directions in this solution are only 19º apart, it is instructive to compare the cumulative delay from two layers to that of the single layer solution. Both in the study of Liu et al. (1995) and in the present study with cross–convolution technique a 1–layer solution delay is very close to the cumulative delay of two layers, when their fast direction are constrained to Liu et al's (1995) values of 79° and 98°. Differences in these cumulative estimates (1.2 s in Liu et al. (1995) vs. 1.5 s in our study) likely result from differences in data sets.

Conclusions

We have developed a waveform fitting technique that allows the testing of shear waves (e.g., SKS and similar phases) for splitting, as predicted by anisotropic earth models. Synthetic tests show that the technique can successfully recover orientation and magnitude parameters for one or more layers of anisotropy, either from individual

seismograms or from suites of observations that include a broad range of backazimuths. The original model is successfully recovered when an appropriate model operator is applied, e.g., when synthetics generated in a 2–layer model are fit with a 2–layer operator. Use of the wrong model leads to a significant degradation of the solution (e.g., as measured by overall variance reduction), making it possible to determine the minimal number of distinct anisotropic layers in a model. Such determinations are always subject to nonuniqueness associated with "cross–polarized" anisotropic layers, since their effects on the waveforms cancel out.

We have tested our technique with a waveform data from station PFO (Piñon Flat, CA), with the following results:

1) Under the assumption of a single layer of anisotropy, our technique yields results similar to other commonly used methods of determining splitting parameters. Furthermore, results obtained with our new technique agree well with previously published findings that were based on different subsets of data.

2) Our new technique identifies a region in the model space of 2–layered anisotropic solutions that contains solutions that are better, in a formal sense, then a one–layered solution. This region includes models with anisotropy directions identified by previous studies by Őzalaybey and Savage (1995), Liu et al. (1995) and Polet and Kanamori (2002). Differences in sets of analyzed data likely lead to deviations in layer–specific delays identified through our method. Our best–fitting two–layer model is of the "nearly one–layer" type.

3) The overall variance reduction of the two–layer fit for PFO is only marginally better for the 2–layer solution than the 1–layer solution (judged to be at the 80% confidence level by the F–test). This results is consistent with the low degrees of significance estimated by Őzalaybey and Savage (1995) and Liu et al. (1995).

The new waveform–fitting method presented here provides means to test whether observed data (e.g. SKS and PKS waveforms) conform to expectations of class of anisotropic earth models (such as the one–layer and two–layer models). In case of the PFO dataset, the misfit is large. The generally poor fit of a one–layer anisotropic model to the PFO data, as judged both by the new method and traditional ones, strongly suggests the presence of some other process is occurring. However, since the two–layer models only minimally improves the fit, this process is probably not dominated by two–layered anisotropy. We have not formally ruled out models with larger number of anisotropic layers, but neither do we believe that attempting to fit the data with models containing a large number of layers will be a fruitfull approach. The whole idea of mantle layering is probably a significant oversimplification of its actual structure, so that if complicated models are indeed to be used, they should probably include the effects of scattering as well as anisotropy.

We reach an overall conclusion that, while waveforms of teleseismic shear waves observed at PFO reflect the presence of anisotropy along their paths, they are also influenced by other processes that are of similar intensity. Consideration of these other processes is of primary concern, as they might strongly influence the outcomes

of shear–wave splitting studies, and bias their interpretation in terms of geodynamic processes.

Acknowledgements. This research was supported by the National Science Foundation grant EAR-9805206 (VL). We thank Jim Gaherty, Martha Savage and John Vidale for helpful comments. Lamont–Doherty Contribution No. 0000.

yyyy.jdy.hr.mn	phase	lat	lon	depth	dist	baz
1992.073.17.41	SKS	39.71	39.6	27	103.41	18.72
1999.316.17.20	SKS	40.76	31.16	10	99.87	24.32
1995.326.04.34	PKS	28.83	34.8	10	111.89	27.01
1995.326.04.38	SKS	28.83	34.8	10	111.89	27.01
1995.166.00.38	SKS	38.4	22.28	14	98.44	31.5
1992.255.04.17	PKS	–6.09	26.65	11	136.14	59.48
1993.270.14.00	SKS	–53.65	–51.62	33	103.65	146.49
1994.169.03.47	SKS	–42.96	171.66	14	100.82	225.08
1993.222.01.14	SKS	–45.28	166.93	28	104.93	225.11
1992.044.01.50	SKS	–15.89	166.32	10	88.54	249.76
1999.095.11.29	SKS	–5.59	149.57	150	96.4	267.52
1997.356.02.27	SKS	–5.5	147.87	179	97.76	268.54
1993.286.02.28	SKS	–5.89	146.02	25	99.51	269.22
1993.298.10.49	SKS	–5.91	145.99	30	99.55	269.22
1998.198.09.12	SKS	–2.96	141.93	10	101.31	273.99
1998.210.18.23	SKS	–2.69	138.9	33	103.67	275.95
1995.079.00.16	SKS	–4.18	135.11	33	107.64	276.86
1992.355.21.16	SKS	–6.58	130.39	78	112.88	277.53
1996.048.06.22	SKS	–0.89	136.95	33	104.27	278.61
1996.048.20.41	SKS	–0.92	136.23	32	104.88	279.01
1996.048.14.44	SKS	–0.57	135.84	19	105	279.54
1992.270.22.39	SKS	1.29	129.12	28	109.38	285.22
1994.153.18.36	PKS	–10.48	112.83	18	129.4	285.27
1993.220.08.56	SKS	12.98	144.8	59	89.94	285.61
1994.021.02.47	SKS	1.01	127.73	20	110.66	285.86
1993.343.04.55	SKS	0.49	126	15	112.36	286.53
1997.329.12.38	SKS	1.24	122.54	24	114.64	289.48
1998.245.09.00	SKS	5.41	126.76	50	108.75	290.19
1996.204.14.43	SKS	1	120.45	33	116.42	290.71
1996.001.08.29	SKS	0.73	119.93	24	117	290.84

1992.138.10.12	SKS	7.24	126.64	33	107.7	291.77
1995.111.00.32	SKS	12.01	125.66	20	105.42	296.26
1995.125.04.16	SKS	12.63	125.3	16	105.29	296.98
1996.163.18.45	SKS	12.61	125.15	33	105.4	297.07
1999.345.18.26	SKS	15.77	119.74	33	107.19	303.17
1995.279.18.29	PKS	–2.04	101.44	33	132.58	303.54
1998.091.18.15	PKS	–0.54	99.26	56	132.95	307.1
1994.144.04.23	SKS	23.96	122.45	16	99.69	307.45
1994.156.01.32	SKS	24.51	121.9	11	99.66	308.21
1995.312.07.33	PKS	1.83	95.05	33	133.79	313.65
1992.232.02.27	SKS	42.14	73.57	27	103.69	352.36

Table 1. Core–refracted shear–polarized phases observed at Piñon Flat during 1992–1999.

method	*delay, s*	*azimuth, deg*
Őzalaybey & Savage, 1995	1.45	89
Liu et al., 1995	1.2	92
Polet & Kanamori, 2002	Not given	Not given
Minimum tangential, fixed initial polarization	0.9	78
Minimum tangential, variable initial polarization	0.9	78
Maximum Cross Correlation	1.1	75
Minimize Cross–Convolution Error	1.5	80

Table 2. One–layer solutions for Station PFO, computed for the whole suite of data.

method	*bottom delay, s*	*bottom azimuth, deg*	*top delay, s*	*top azimuth, deg*	*variance reduction, %*
One–layer cross convolution	1.5	80			55.46
Two–layer cross–convolution	3.0	69	1.8	152	57.09
Őzalaybey & Savage (1995)	1.2	70	0.60	110	
Liu et al., (1995)	0.5	79	0.70	98	
Polet and kanamori (2002)	1.2	80	0.50	140	
Sub–optimal (#1) two–layer cross–convolution	1.4	70	0.40	110	56.36
Sub–optimal (#2) two–layer cross–convolution	1.4	79	0.20	98	55.68

Table 3. One–layer and two–layer solutions for Station PFO. Variances reduction are given relative to the case of no anisotropy. The sub–optimal solutions 1 and 2 constrain the axes to the directions given by Őzalaybey & Savage (1995) and Liu et al. (1995), respectively.

References

Anderson D. L., and A. M. Dziewonski, 1982. Upper mantle anisotropy; evidence from free oscillations, Geophysical Journal of the Royal Astronomical Society. 69, 383–404.

V. Babuska, M. Cara, 1991. Seismic Anisotropy in the Earth, Kluwer Academic, Dordrecht.

Ben Ismail, W. and D. Mainprice, 1998. An olivine fabric database; an overview of upper mantle fabrics and seismic anisotropy, Tectonophysics. 296, 145–157.

Burdick, L. and C. Lanston, 1977. Modeling crustal structure through the use of converted phases in teleseismic body–wave forms, Bull. Seism. Soc. Am. 67, 677–691.

Burlini, L. and D. Fountain, 1993. Seismic anisotropy of metapelites from the Ivrea–Verbano Zone and Serie dei Laghi (northern Italy). Phys. Earth Planet. Interiors 78, 301–317.

Christensen, N. I., 1984. The magnitude, symmetry and origin of upper mantle anisotropy based on fabric analyses of ultramafic tectonites, Geophys. J. Roy.l Astr. Soc. 76, 89–111.

Creager, K. C., 2000. Inner core anisotropy and rotation. Geophysical Monograph, American Geophysical Union 117, 89–114.

Hartog, R., S. Y. Schwartz, 2000. Subduction–induced strain in the upper mantle east of the Mendocino triple junction, California. J. Geophys. Res. 105 , 7909.

Holliger, K. and A. Levander, 1994. Lower crustal reflectivity modeled by rheological controls on mafic intrusions. Geology 22, 367–370.

Kaminski, E. and N. M. Ribe, 2001. A kinematic model for recrystallization and texture development in olivine polycrystals. Earth Planet. Sci. Lett.s. 189, 253–267.

Kendall, J. M. and P. G. Silver, 1998. Investigation of causes of D" anisotropy.Geodynamics Series. 28, 97–118.

Liu, H., P. M. Davis and S. Gao, 1995. SKS splitting beneath southern California, Geophys. Res. Lett. 22, 67–770, 1995.

Levin, V., W. Menke and J. Park, 1999. Shear–wave splitting in Appalachians and Urals: a case for multilayered anisotropy, J. Geophys. Res. 104, 17,975–17,994.

Mellman, G.R, 1980. A method of body-wave waveform inversion for the determination of Earth structure, Geophys. J.R. Astr. Soc. 62, 481-504.

Menke, W., 1989. Geophysical Data Analysis: Discrete Inverse Theory, Revised Edition (textbook), Academic Press, Inc., New York.

Menke, W., 2000. SPLITTING MODELER Software, ftp: //ftp.ldeo.columbia.edu/pub/menke/SPLITTING_MODELER.tar.Z.

Montagner, J.–P., 1998. Where can seismic anisotropy be detected in the Earth's mantle?, Pure Appl. Geophys. 151, 2–4.

Özalaybey, S., and M. Savage, 1995. Shear–wave splitting beneath western United States in relation to plate tectonics, J. Geophys. Res. 100, 18,135–18,149.

Park, J., and V. Levin, 2002. Seismic anisotropy: Tracing plate dynamics in the mantle, Science, in press.

Phinney, R., 1964. Structure of the Earth's crust from spectral behavior of long–period body waves, J. Geophys. Res. 69, 2997–3017.

Polet, J. and H. Kanamori, 2002. Anisotropy beneath California: shear wave splitting measurements using a dense broadband array, Geophys. J. Int. 149, 313–327.

Rümpker, G. and P. G. Silver, 1998. Apparent shear–waves splitting parameters in the presence of vertically varying anisotropy. Geophys. J. Int., 135, 790.

Savage, M., 1999. Seismic anisotropy and mantle deformation; what have we learned from shear wave splitting?. Rev. of Geophys. 37, 65–105.

Saltzer, R.L., J. B. Gaherty, T. H. Jordan, How are shear–wave splitting measurements affected by variations in the anisotropy with depth?. Geophys. J. Int., 141, 374, 2000

Silver, P. G., 1996. Seismic anisotropy beneath the continents: Probing the depths of geology, Ann. Rev. Earth Planet. Sci., 24,385–432.

Silver, P. G., and W. W. Chan, 1991. Shear–wave splitting and subcontinental mantle deformation, J. Geophys. Res. 96, 16,429–16,454.

Silver, P.G. and M. K. Savage, 1994. The interpretation of shear–wave splitting parameters in the presence of two anisotropic layers. Geophys. J. Int., 119, 949.

Vinnik, L.P., G.L. Kosarev and L.I. Makeyeva, 1984. Anisotropy of the lithosphere according to the observations of SKS and SKKS waves (in Russian), Doklady Akademii Nauk SSSR 278, 1335

Vinnik L.P., L.I. Makeyeva, A. Milev and A. Yu. Usenko, 1992. Global patterns of azimuthal anisotropy and deformations in the continental mantle. Geophys. J. Int..

111, 433–447.

Zhang, S. and Karato, S., 1995. Lattice preferred orientation of olivine aggregates deformed in simple shear, Nature 375, 774–777.

This Page is Left Intentionally Blank

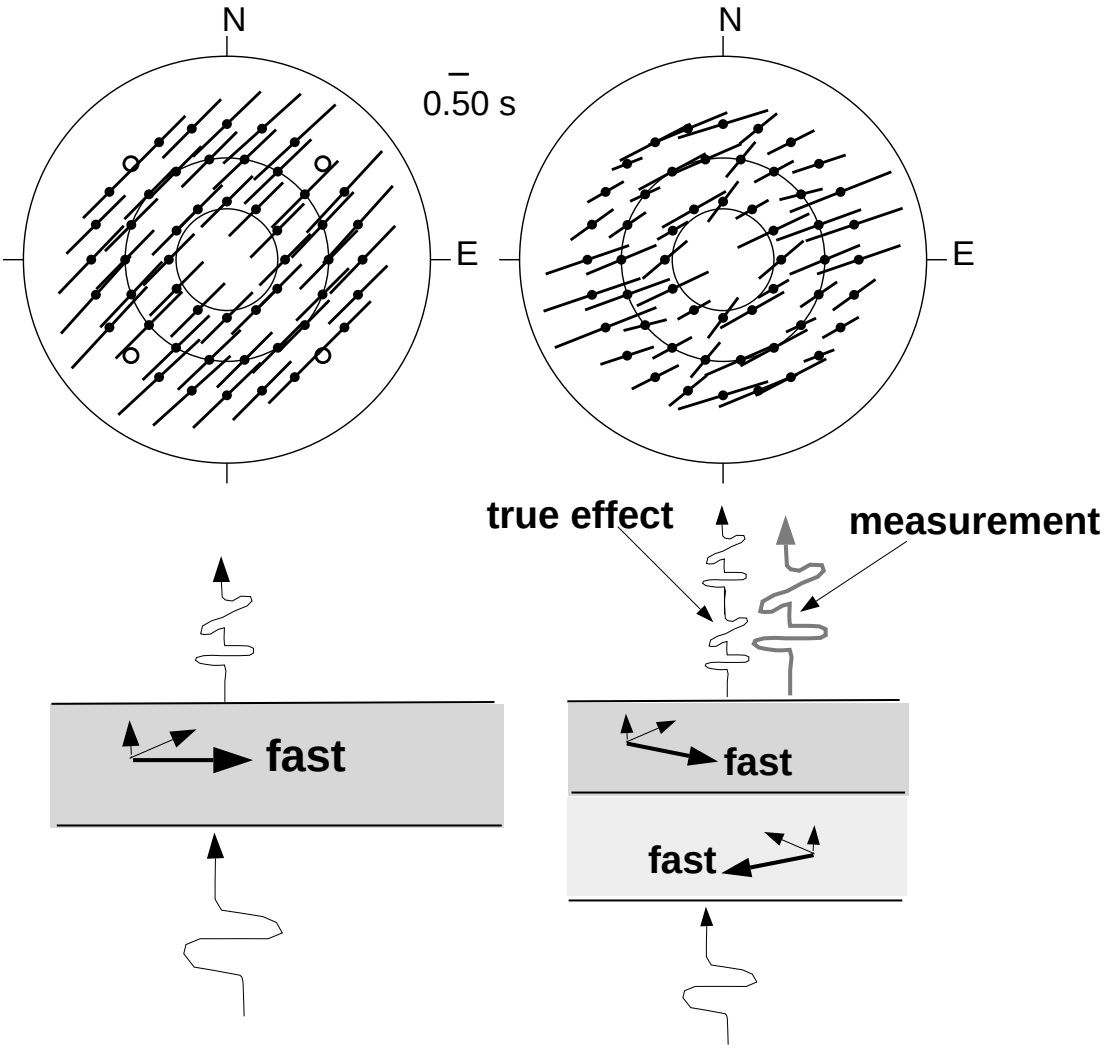

Fig. 1. Shear wave splitting in one and two–layer media. Bottom left: A linearly polarized shear wave pulse enters an anisotropic layer and is split into two components that propagate at different velocities. The polarization direction of the faster component is parallel to the fast anisotropic axis of the layer. Top Left: Graphical depiction of the splitting parameters for radially–polarized shear waves of different backazimuths, ϕ, and angles of incidence. The orientation of the line segment indicates fast azimuth azimuth, θ, and its length is proportional to delay time, τ. The position of the line segment on the polar diagram indicates backazimuth and angle of incidence, with the 10, 20 and 40 km/s circles shown.. Note that with the exception of a few "null" directions (circles) where splitting parameters cannot be determined, all the estimates are similar. Bottom right: Two–layer case. The true response has four pulses. The "apparent splitting" method approximates these four pulses with a best–fitting set of two pulses. Top tight: The resulting pattern of estimated apparent splitting parameters varies strongly with backazimuth. See Levin et al. (1999) for a detailed description of the anisotropic models.

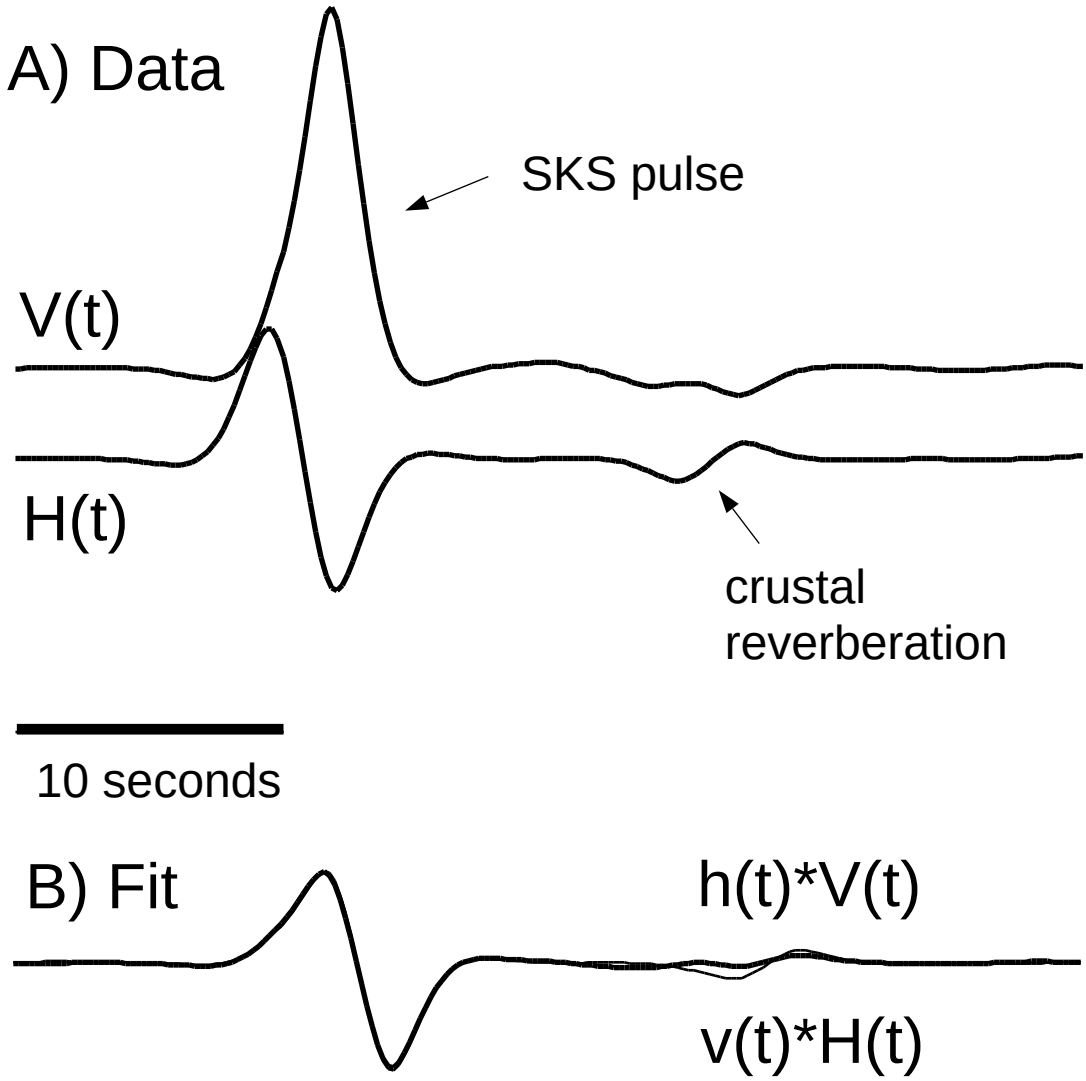

Fig. 2. A) Synthetic seismograms for an earth model with one anisotropic layer. Radial–horizontal, V(t), and tangential–horizontal, H(t) components for a backazimuth of ϕ=0° are shown. B) The fit obtained by the one–layer cross–convolution modeling procedure is excellent.

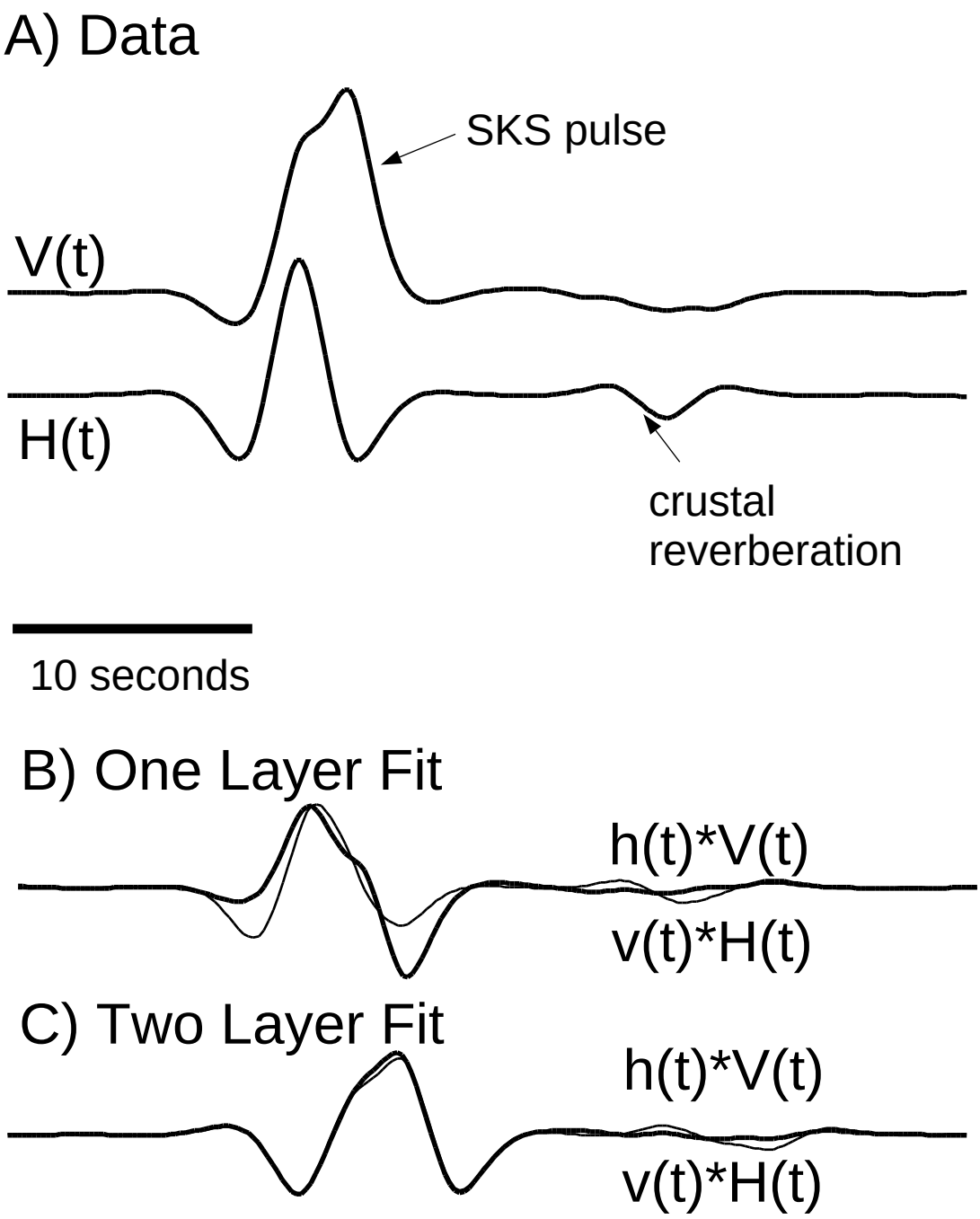

Fig. 3. A) Synthetic seismograms for an earth model with two anisotropic layers. Radial–horizontal, V(t), and tangential–horizontal, H(t) components for a backazimuth of ϕ=0° are shown. B) The fit obtained by the one–layer cross–convolution modeling procedure is poor. C) The corresponding two–layer fit is excellent.

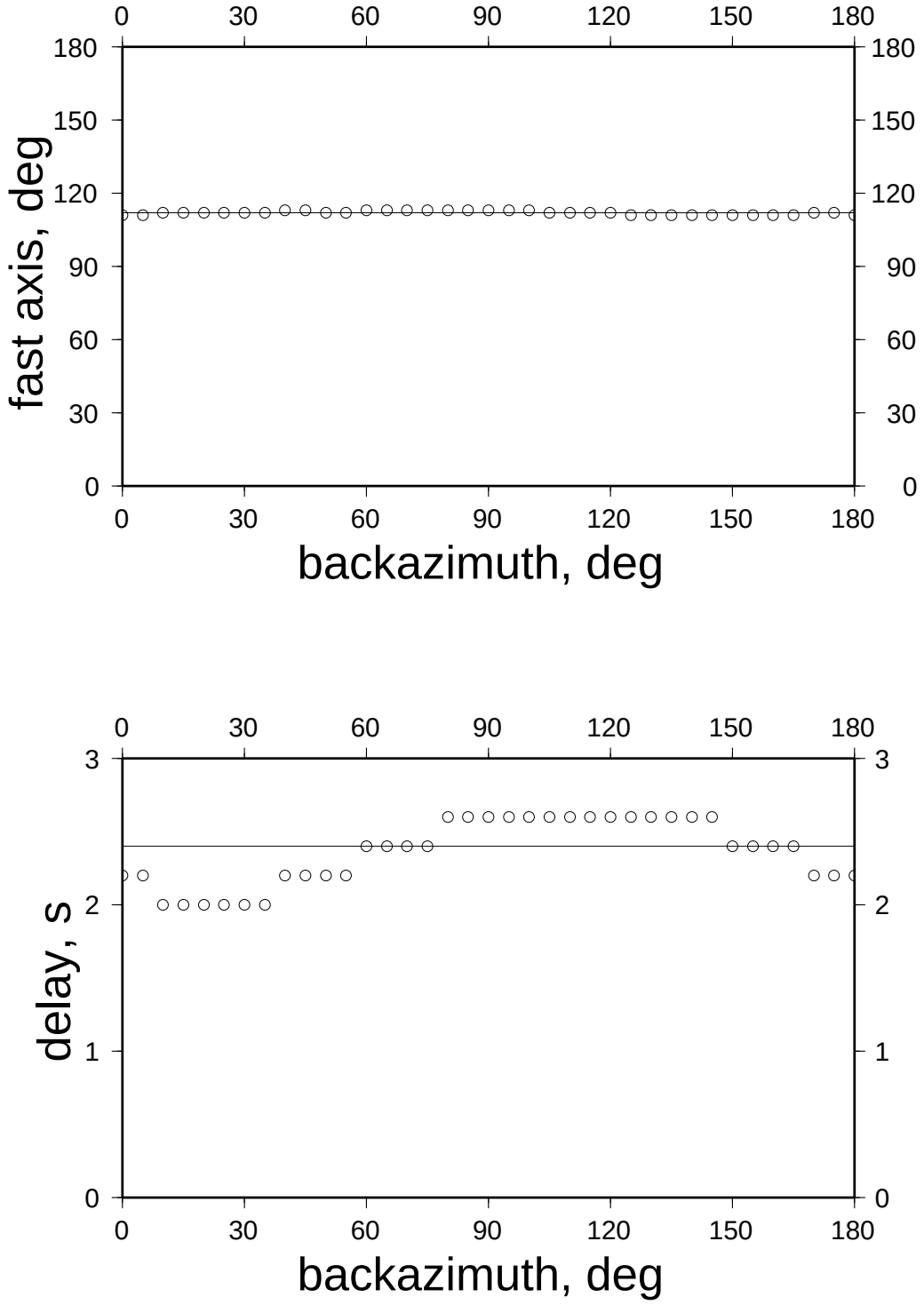

Fig 4. Results of one–layer cross–convolution method applied to synthetic data calculated from an earth model with one anisotropic layer. Top: Estimated azimuth, θ, of the fast axis vs. backazimuth, ϕ. Bottom. Estimated delay, τ, vs. backazimuth. Lines depict the whole–suite estimates, circles, the individual seismogram estimates.

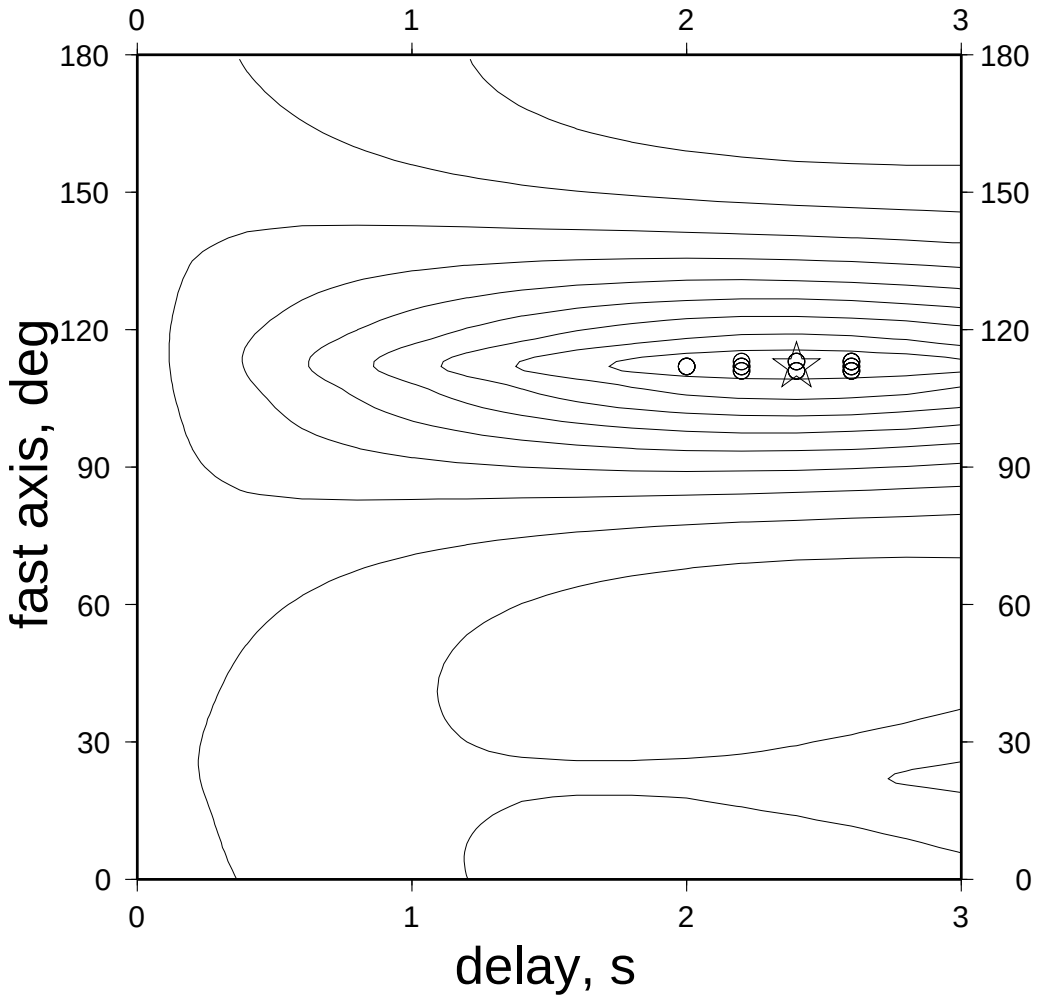

Fig 5. Whole−suite error surface for the one−layer cross−convolution method appied to synthetic seismograms from the one anisotropic layer model. Star: global minimum.Circles: Individual seismogram estimates.

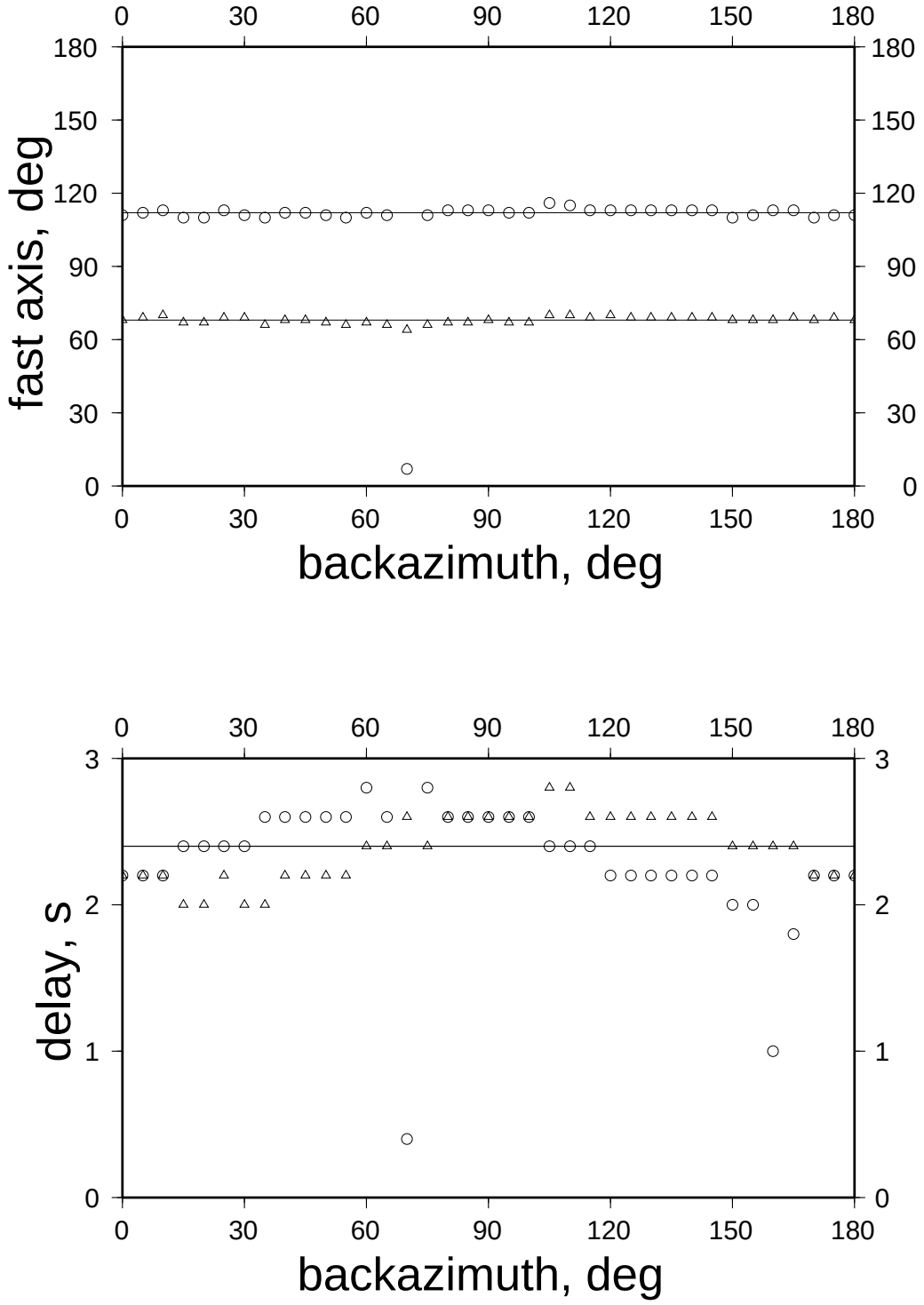

Fig. 6. Results of two–layer cross–convolution method applied to synthetic data calculated from earth model with two anisotropic layers. Top: Estimated azimuths, θ and ψ, of the fast axes of the bottom and top layers vs. backazimuth, ϕ. Bottom. Estimated delays, τ_1 and τ_2, vs. backazimuth. Lines depict whole–suite estimates, circles and triangles, the individual seismogram estimates.

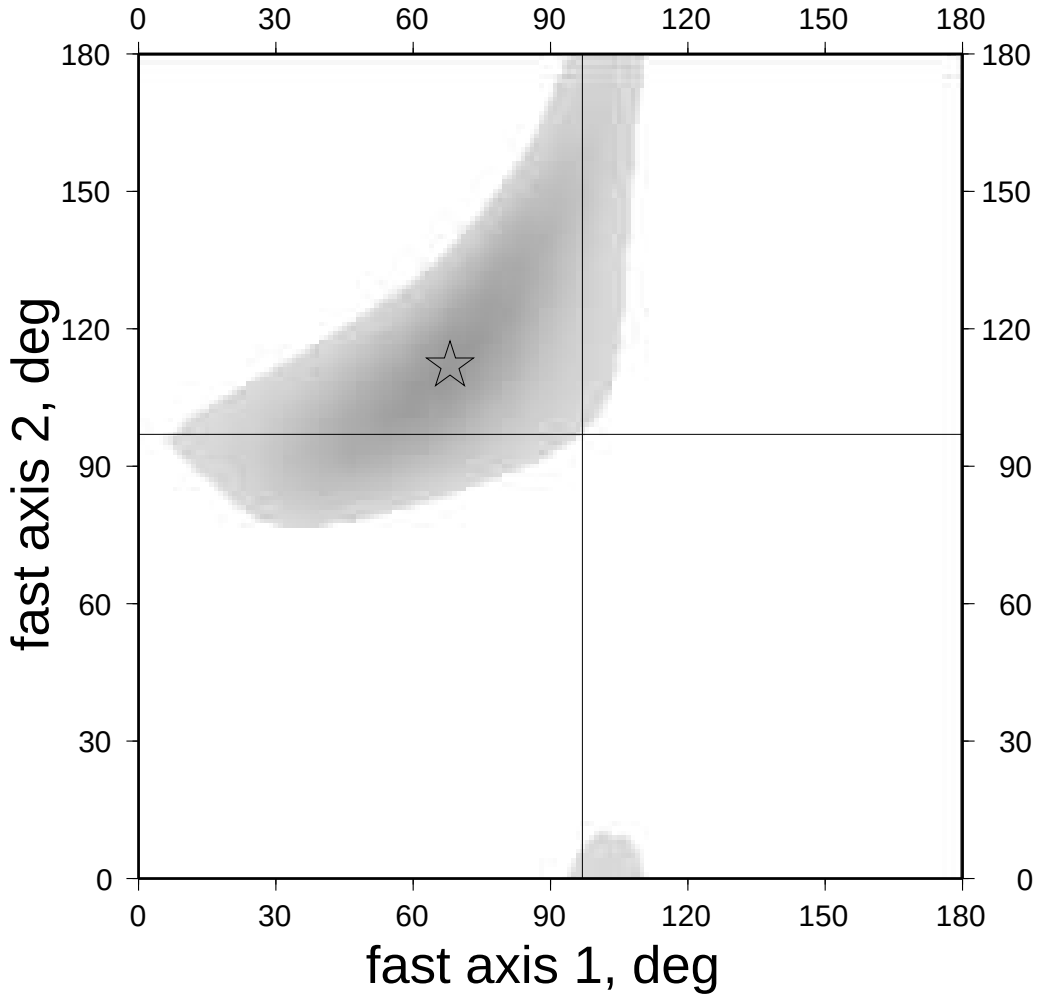

Fig 7. Whole–suite error surface for the two–layer cross–convolution method applied to synthetic seismograms from the two anisotropic layer earth model. All regions where the error is greater than the best–fitting one–layer solution are shown in white. Darker shades correspond to smaller errors. Star: global minimum.

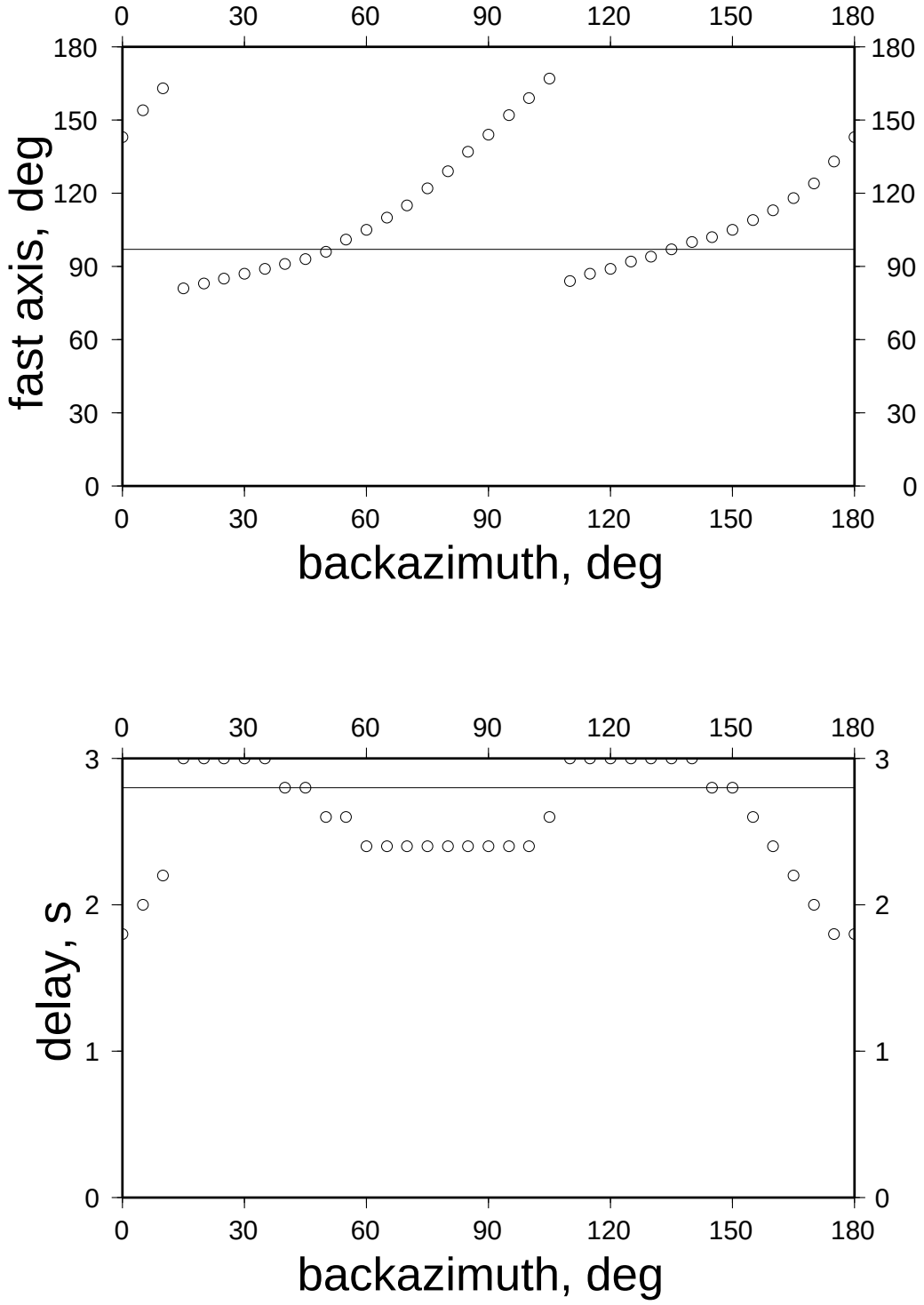

Fig. 8. Results of the one–layer cross–convolution method applied to synthetic data calculated from earth model with two anisotropic layer. Top: Estimated azimuth, θ, of the fast axis vs. backazimuth, ϕ. Bottom. Estimated delay, τ, vs. backazimuth. Lines depict the whole–suite estimates, circles, the individual seismogram estimates. Note the “sawtooth” pattern in the individual seismogram fast–axis estimates.

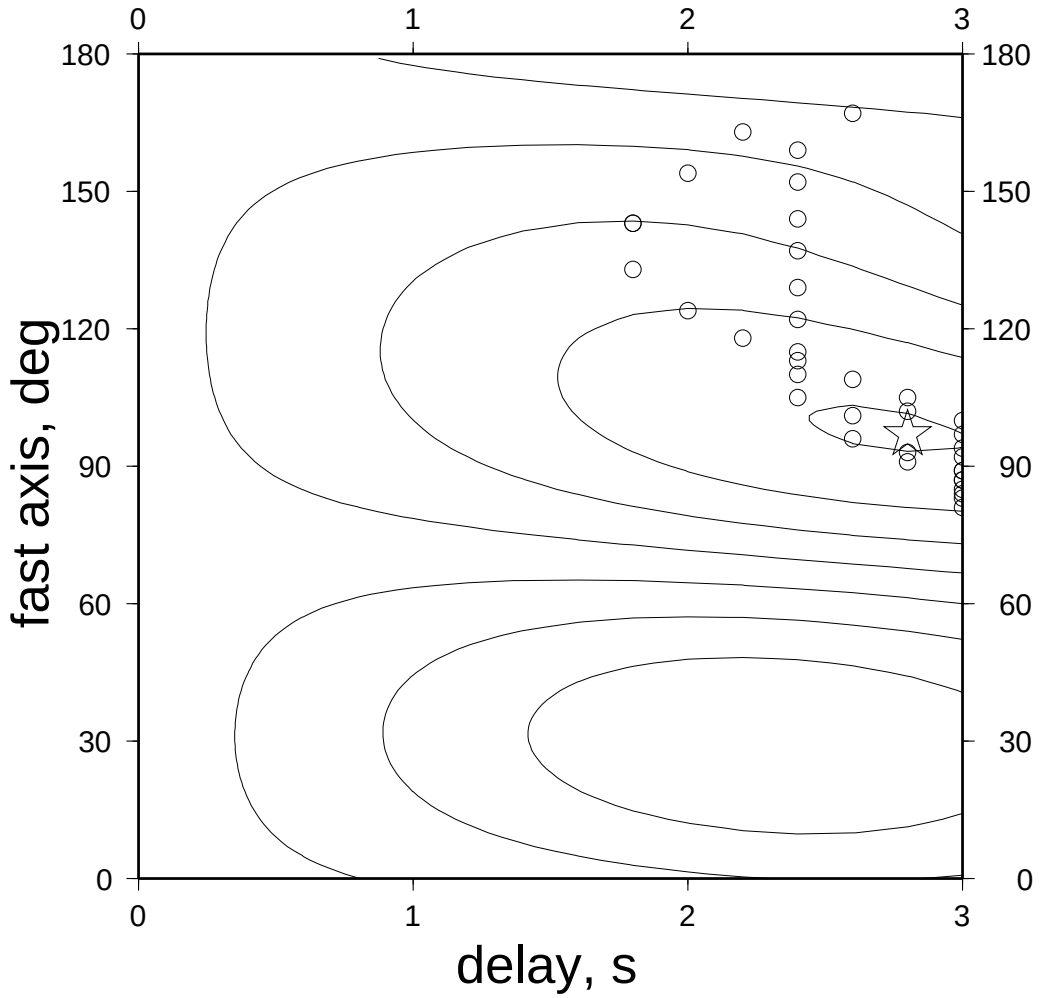

Fig. 9. Whole−suite error surface for the one−layer cross−convolution method applied to synthetic seismograms from the two anisotropic layers earth model. Star: global minimum.Circles: Individual seismogram estimates. Note wide scatter of individual estimates.

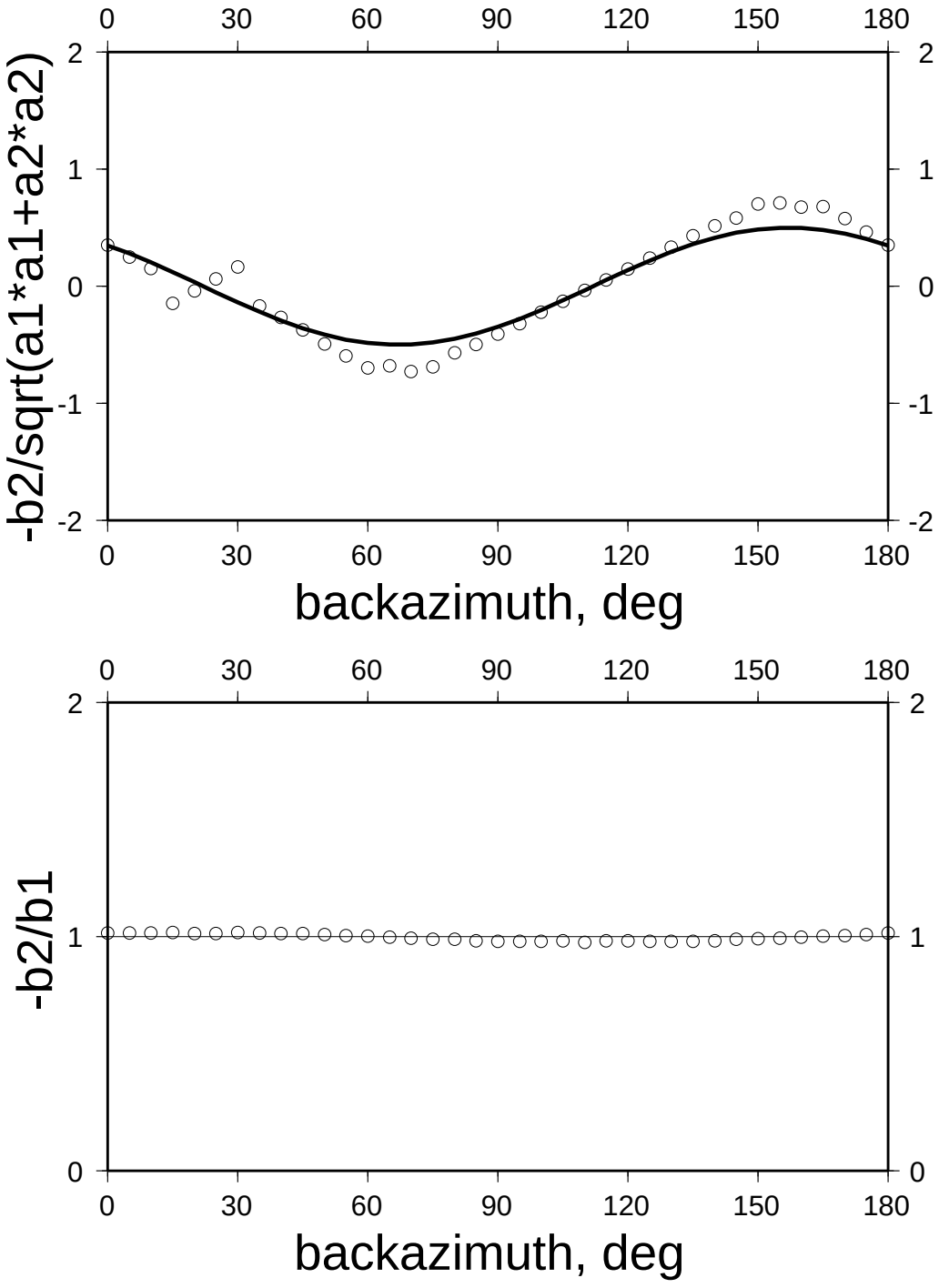

Fig 10. Tests of conformance to a one–layer interpretation, which uses the results of the two–pulse operator method. Lines: predicted values. Circles: Values estimated from individual synthetic seismograms from one anisotropic layer earth model. See text for further discussion.

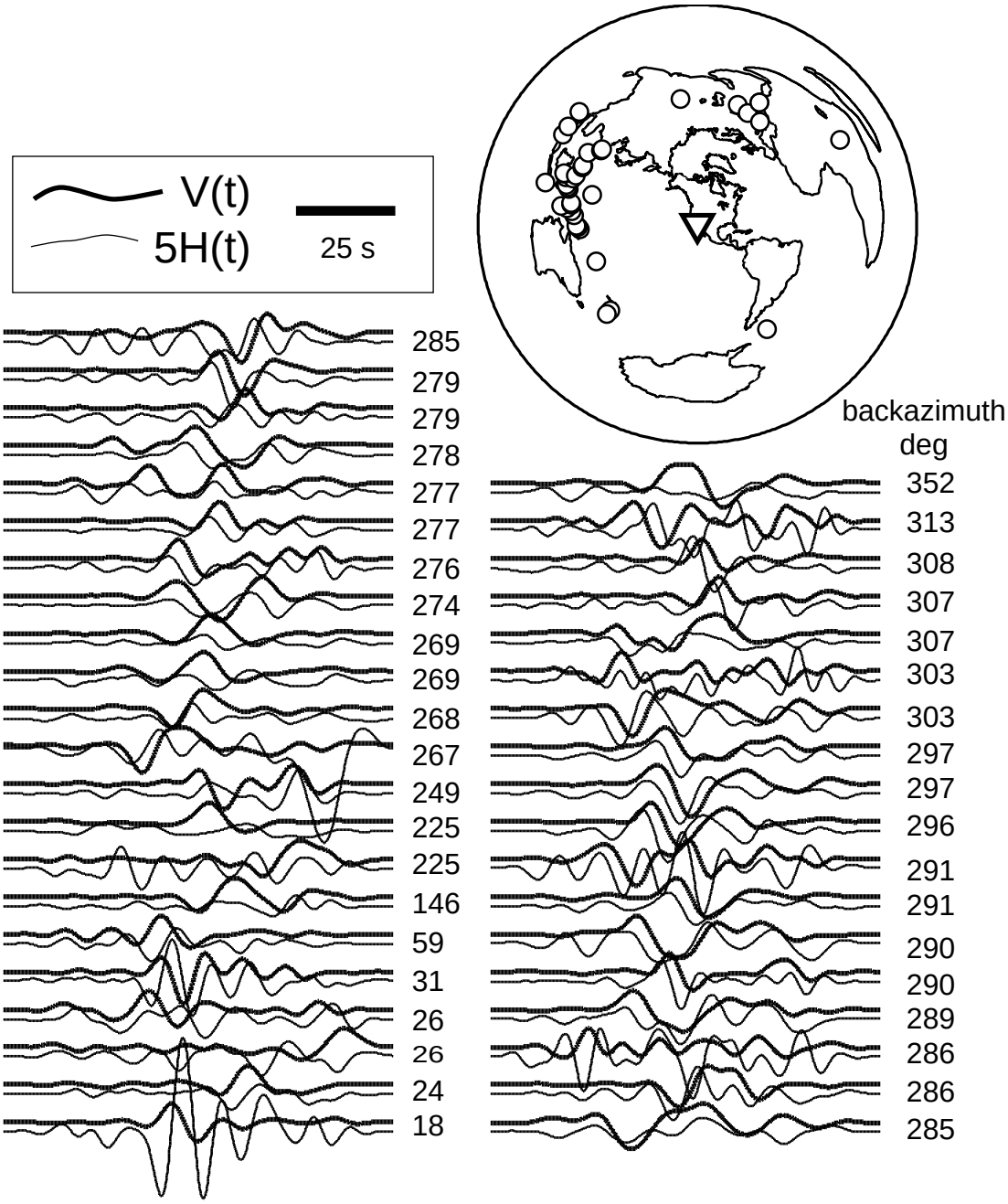

Fig 11. Radial–horizontal component, V(t), (bold) and tangential–horizontal component, H(t), (solid) from 41 earthquake sources with a broad range of backazimuths, ϕ. Note that the scale of the two components differ by a factor of 5. Inset: Map of sources (circles) centered on PFO (triangle).

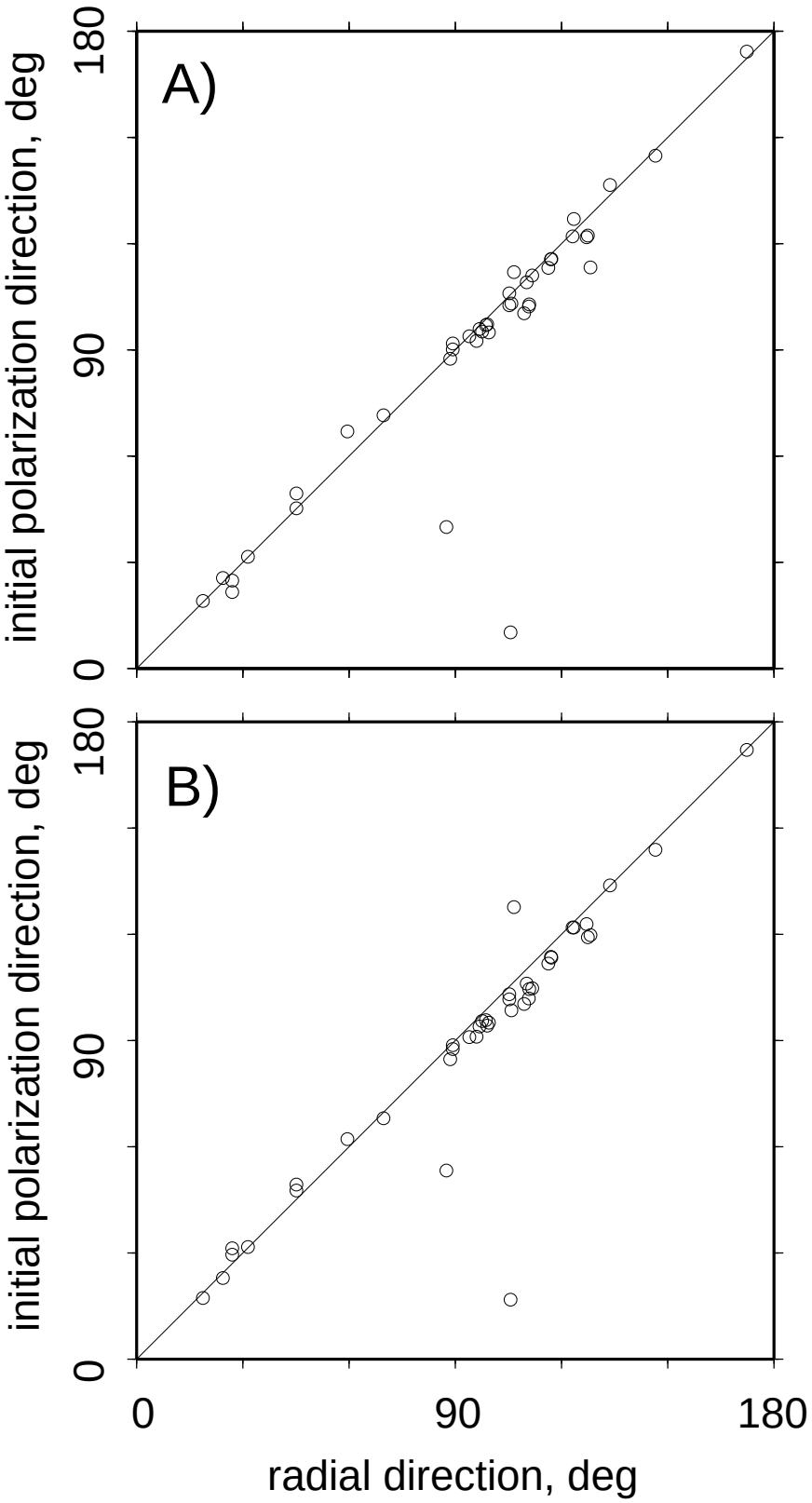

Fig. 12. Azimuth of the initial polarization direction (circles) at station PFO, compared with the expected radial direction (line). A) Method B. B) Method C.

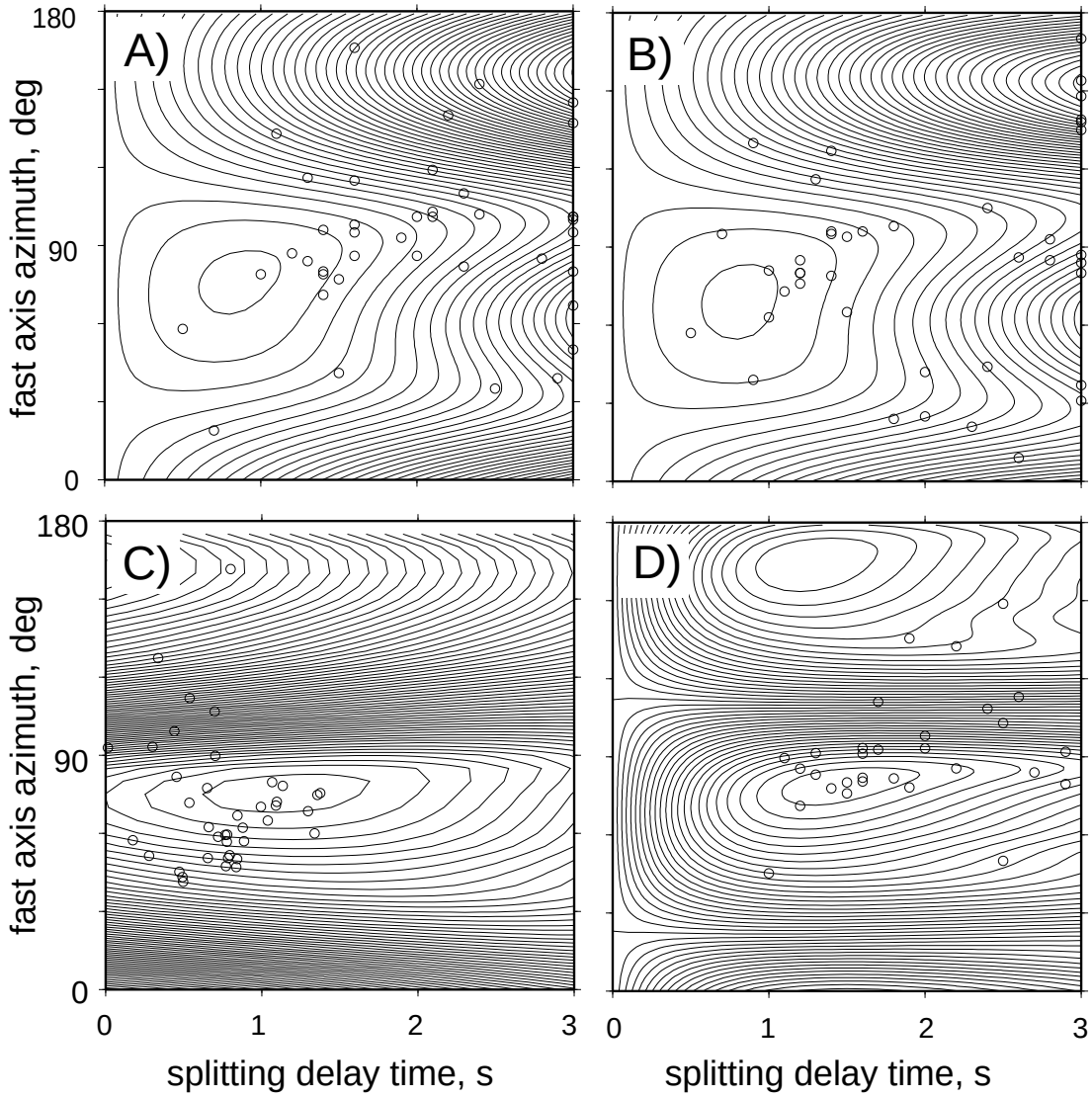

Fig. 13. Whole–suite error surfaces (contours) for several methods for estimating one–layer splitting parameters, with individual–seismogram estimates (circles). A) Minimum tangential component method with fixed initial polarization. B) Minimum tangential component method with variable initial polarization. C) Maximum cross–correlation method. D) Cross–convolution method.

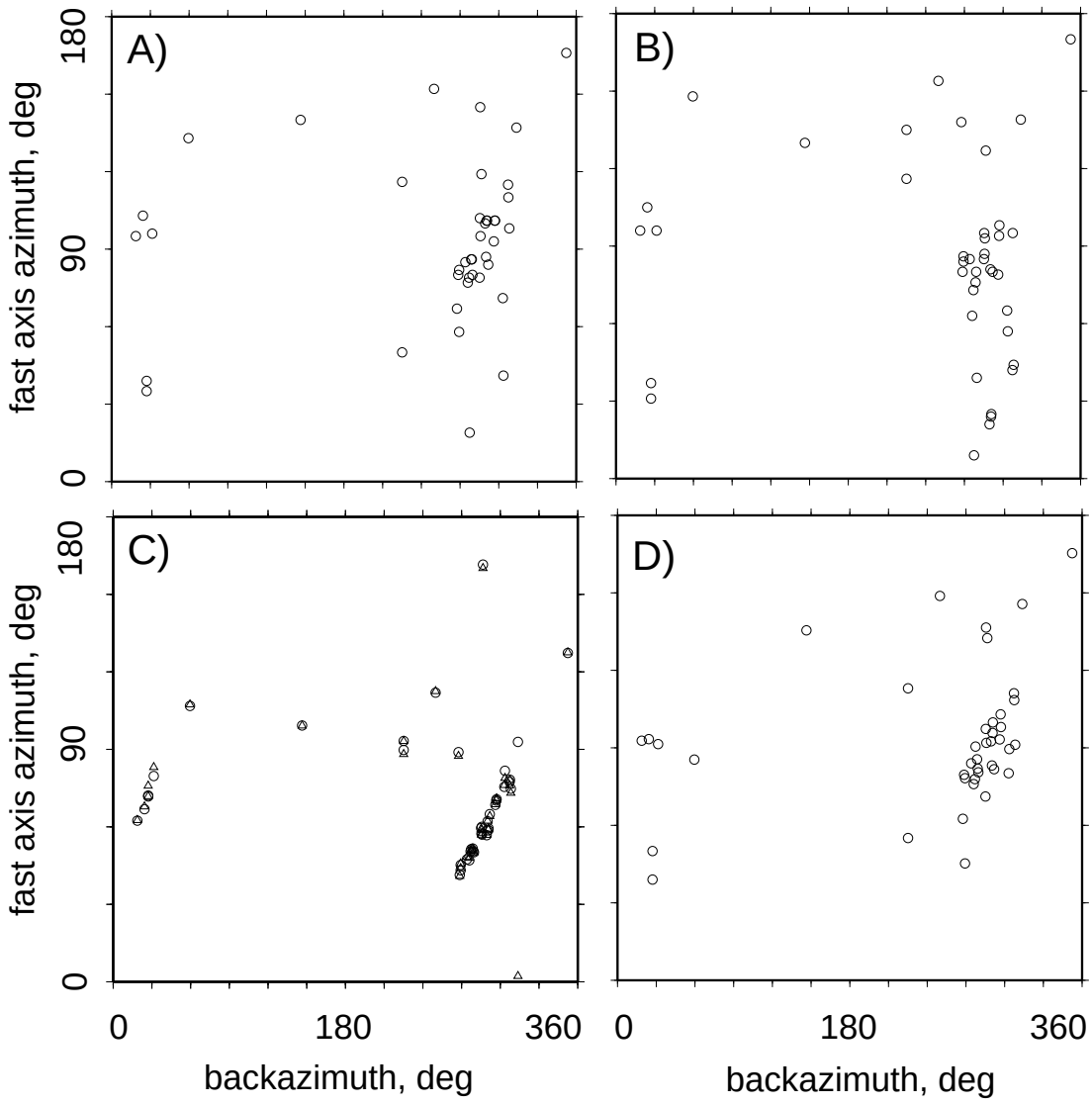

Fig. 14. One–layer estimates of the azimuth, θ, of the fast axis at PFO vs. backazimuth, ϕ, of the source. A) Method A. B) Method B. C) Method C. D) Method D. Note “sawtooth” pattern.

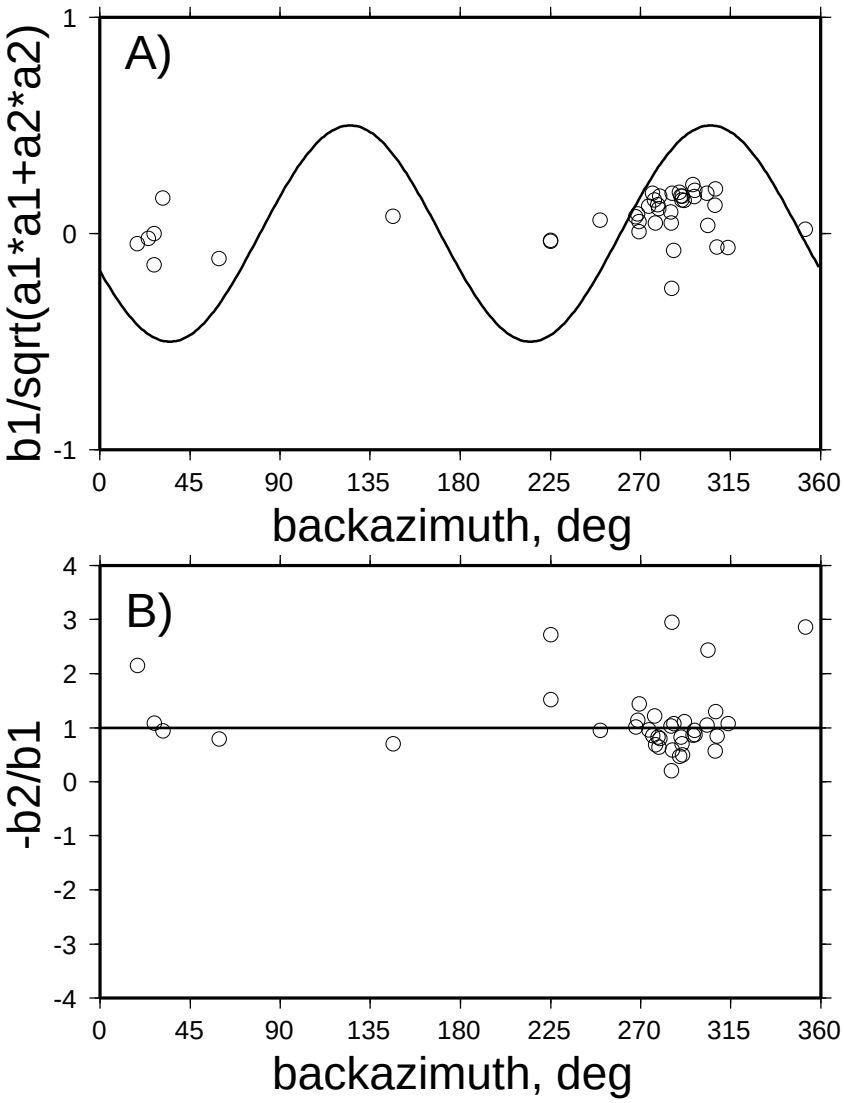

Fig 15. Tests of conformance to a one–layer interpretation, that uses the results of the two–pulse operator method. Lines: predicted values. Circles: Values estimated from individual PFO seismograms. See text for further discussion.

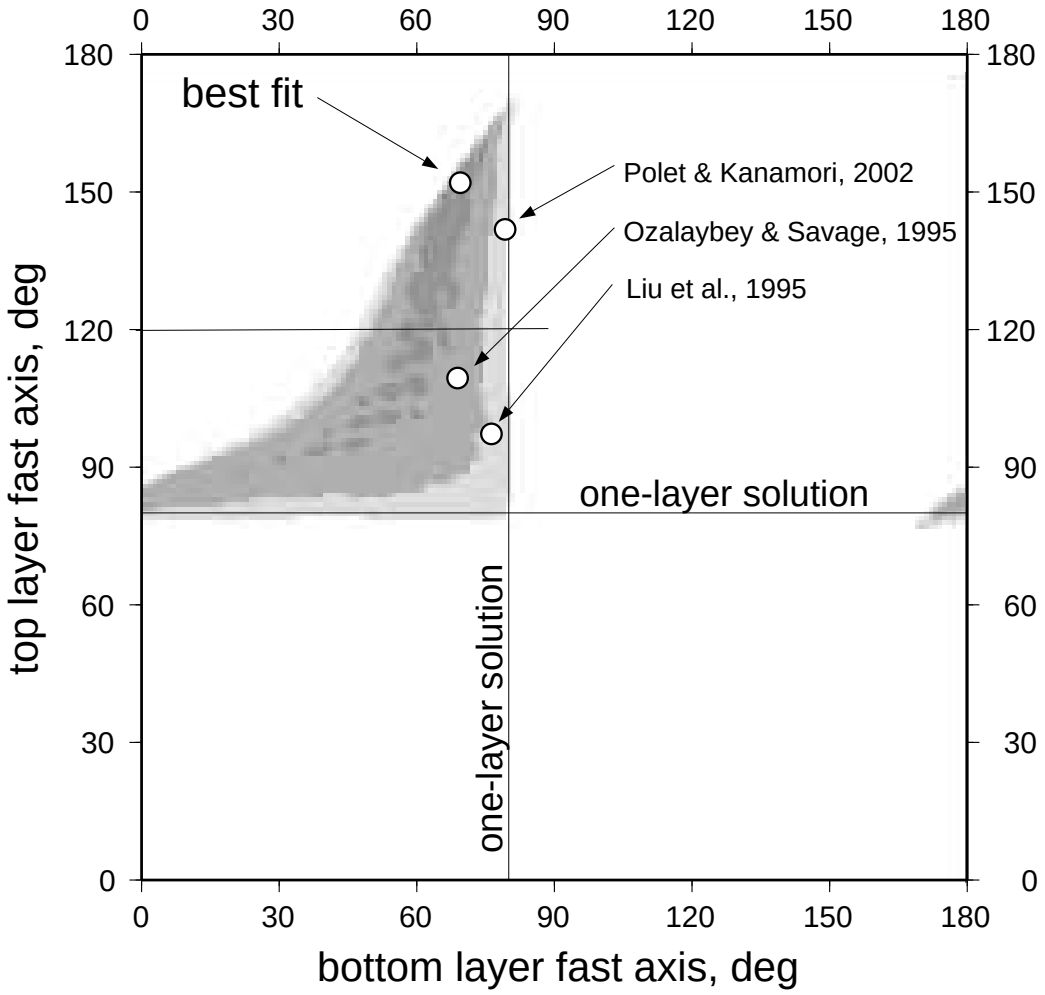

Fig. 16. Whole–suite error surface for two–layer cross–convolution method, as a function of the azimuth of the fast axes of the two anisotropic layers. All regions where the error is greater than the best–fitting one–layer solution is shown in white. Darker shades correspond to smaller errors.